POLITECNICO DI MILANO

Corso di Laurea MAGISTRALE in Ingegneria dell'Automazione

Scuola di Ingegneria Industriale e dell'Informazione

RAILWAY BOGIE STABILITY CONTROL FROM SECONDARY YAW ACTUATORS

Relatore: Prof. Stefano BRUNI (Politecnico di Milano)

Correlatore: Prof. Roger GOODALL (Loughborough University)

Correlatore: Ing. Christopher WARD (Loughborough University)

Correlatore: Ing. Stefano ALFI (Politecnico di Milano)

Tesi di Laurea di:

Davide PRANDI, matricola 801231

Anno Accademico 2013-2014

Contents

List of Figures

List of Tables

Abstract

Thanks to the continuos development of control technology, in the last two decades the study on active systems in the railway field has been increasing. Active systems, but in general active control, have been developed in different ways all over the world taking into account the need of specific situations, mainly to improve performances on the existing infrastructures. The objectives in this direction are, briefly, faster travelling speed without loss in passenger comfort and better handling performances.

The aim of this thesis is to overcome the trade-off between stability in straight track and curving capability, that is a typical mechanical design limit of a passive railway vehicle. In this sense, active control is here implemented as a controllable yaw torque between the two bogies and the carbody. The idea, that has been studied both theoretically and experimentally, is extended by examining active stabilisation strategies for a bogie with very soft yaw springs between the bogie frame and the wheelsets. The low stiffness connections mean that curving is intrinsically good, but the bogie will be very unstable, hence the use of active control to provide stability.

This work presents two different control strategies, developed on a linear, half vehicle plan view model. The first one is a full state LQ regulator, in the case where all the state are supposed to be perfectly measured. The second is an LQG control with state estimation, taking into account a realistic situation with a set of sensors mounted on the vehicle. Then the results are compared with the fully passive system on a multi body simulator in different operating situations: straight track, in order to validate the control strategy, and then in curved track, to assess the low primary yaw stiffness advantages.

Abstract in italiano

Grazie al continuo sviluppo della tecnologia del controllo, lo studio di sistemi attivi nel campo ferroviario ha avuto un notevole incremento negli ultimi due decenni. I sistemi attivi, ma pi in generale il controllo attivo, sono stati sviluppati in diverse modi ovunque nel mondo, tenendo in considerazione le pi diverse esigenze contingenti, soprattutto con lo scopo di migliorare le prestazioni sfruttando le infrastrutture esistenti. In sintesi, lobiettivo in questo senso un minore tempo di viaggio, abbinato al mantenimento del comfort di viaggio per i passeggeri e a una migliore maneggevolezza della guida. Lobiettivo di questa tesi di superare lo scarto tra la stabilit del veicolo lungo tratti rettilinei e la capacit in curva, che rappresenta un classico problema di progettazione meccanica dei veicoli ferroviari. In questo senso, il controllo attivo viene qui implementato come una coppia di serpeggio tra il singolo carrello e la cassa. Lidea, studiata sia teoricamente sia sperimentalmente [1,2], viene estesa esaminando alcune strategie di stabilizzazione attiva per un carrello con bassa rigidezza primaria di serpeggio. La scarsa rigidezza delle connessioni implica intrinsecamente una buona capacit di curva; il carrello risulta invece instabile, da cui la necessit di utilizzare un controllo attivo per riportare le condizioni di stabilit. Questo lavoro presenta due diverse strategie di controllo, sviluppate su un modello lineare di met veicolo. La prima strategia e' un controllo LQ applicato supponendo che tutti gli stati siano perfettamente accessibili. La seconda un controllo di tipo LQG con stima degli stati; questa seconda strategia permette di prendere in considerazione situazioni pi realistiche grazie all'uso di alcuni sensori montati sul veicolo. I risultati ottenuti vengono confrontati con quelli forniti dal sis-

tema su di un simulatore multi-body, operante in diverse situazioni: tratti con tracciato rettilineo, per validare la strategia di controllo, quindi tratti curvilinei, al fine di dimostrare i vantaggi della ridotta rigidezza primaria di serpeggio.

Chapter 1

Introduction

1.1 Preface

In high speed railway vehicles, the use of active control and active systems has increased in order to overcome certain limits imposed by the mechanical design. One of the most famous examples is the *Pendolino* train, developed by Fiat Ferroviaria in Italy; this is the first example of actively actuated tilting train.

From this initial and successful idea, different applications of active systems on railway vehicles have been studied and developed. This trend of replacing passive components with active systems will continue probably until a radical mechanical redesign of the railway vehicle will be achieved ([5]). Generally, active systems pemit to improve the performances of a certain mechanical system. A typical limit of performances in a railway vehicle is set by the trade-off between critical speed and dynamic stability. Different solutions have been studied over the years, in different countries for specific issues resolution. When the critical velocity is exceeded, a specific kind of dynamic instability occours: the hunting instability. Basically, this phenomenon is caused by the yaw motion of the wheelsets and the bogie, coupled with the wheel-rail contact (Figure 1.2). Active control is intended to overtake the velocity limit, ensuring the dynamic stability.
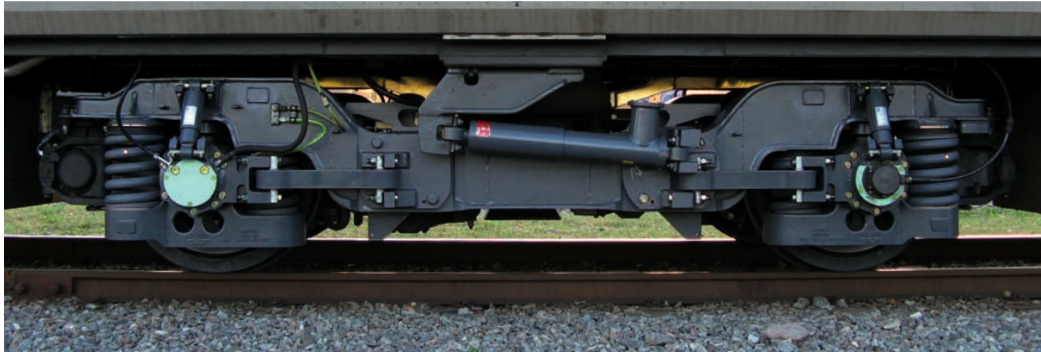
Figure 1.1: Anti yaw damper mounted between the railway bogie and the carbody

This thesis concerns about the active control applied on a secondary suspension, the anti yaw damper. Historically, the anti yaw damper (Figure 1.1) was added to the railway vehicle exactly to dissipate the energy accumulated in the hunting instability phenomenon. Nowadays, with only a few particular exceptions, the totality of long distance passenger vehicles mount this damper.

With this configuration, the vehicle has got its own critical velocity, defined by a number of parameters, affected also by the primary yaw stiffness. This component concerns to the equivalent yaw stiffness of the single wheelset: it comes from a combination of the vertical springs and the bushing stiffness; a physical spring is not present. In simple words, primary yaw stiffness represents the tendency of counteract the wheelset yaw movements. High values of primary yaw stiffness mean an high contrast of the yaw movement; on the opposite, low values mean low contrast.

 Clearly, hunting instability occours with a lower critical speed when primary yaw stiffness is low. On the other hand, a low value of primary yaw stiffness plays a positive role in curving capability.

A soft connection permits to the wheelset to better follow the curved track: this results in reduced wheel-rail creep forces. These forces are generated from a non zero region of contact between wheel and rail; practically, a little elliptical region of the iron is flattened. This results in the fact that the wheel does not advance as far as would be expected from rolling contact. Mainly,

Figure 1.2: Hunting motion: the center of motion of the wheelset describes a sinusoidal path

creep forces can be divided in three different categories:

- Lateral creep forces

- Longitudinal creep forces

- Spin creep forces

These contact forces describe the adhesion and the slip behaviour of the wheel. As a consequence, these forces are the cause of dissipation, because of the non pure rolling situation. Therefore, an undesired component of wear between wheel and rail occours.

The aim of a low primary stiffness connection refers to the concept of "perfect curving" ([3]), that means:

- Equal lateral creep forces for all wheelsets (or equal angle of attack)

- No longitudinal creep forces (or equal creep between two wheels)

In general, spin creep coefficient is small; in the mechanical modellization of this work is set to zero.

Getting close to the concept of perfect curving, the dissipations are reduced, and then the undesired wear. Therefore, a soft primary connection lowers the wear of the wheels and the rails, with various benefits. Two of these benefits are, for example, the extended maintenance time for wheel reprofiling and the extended lifespan of the rails. Moreover, perfect curving completely avoids flange contact, resulting in substantial reduction of wheel-rail wear (Figure 1.3).
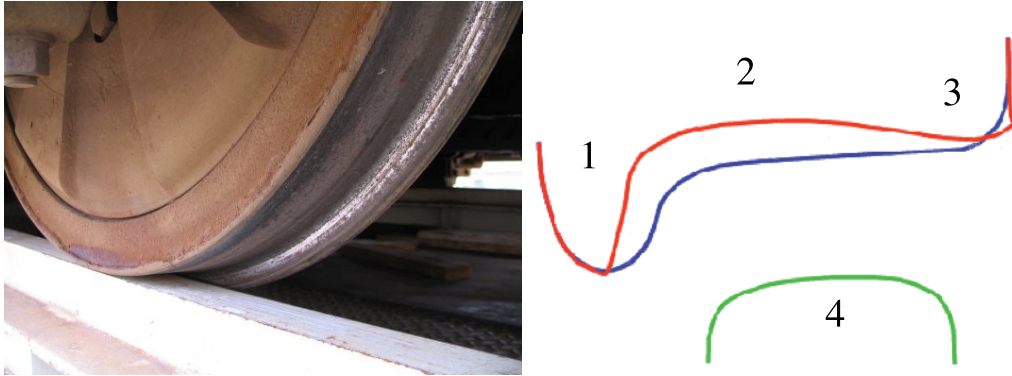
Figure 1.3: Example of wheel wear: on the left, a worn wheel. On the right, the areas of wear: 1) flange wear 2) tread wear 3) false flange 4) unworn rail. Blue line refers to an unworn wheel profile

The aim of the thesis concerns the overcoming of this mechanical trade-off: to reduce the wear through a reduced primary yaw stiffness connection, maintaining the same critical speed. Since, as previously explained, this situation carries to a dynamical instability, the proposed solution is the application of an active control in order to recover the stability situation. In particular, the active control is applied on the secondary yaw suspension: this appoach is called "Secondary Yaw Control" ([3]). Practically, this method is realized replacing the anti-yaw dampers with an electric motor equipped with a proper transmission, that permits to convert the rotational to the linear movement. The description of these phenomena, in particular the contact forces, could become difficult when an accurate discussion is needed. In order to avoid unnecessary complications, the active control strategies have been developed on a linear model; then, the results have been validated on a multi body non linear model. In this way, it is possible to evaluate, with a good accurancy, the creep forces and to compare them in every single situation.

Considering this scenario, an initial guess of primary yaw stiffness reduction has been done; then, through an appropriate lineal model, the passive and the active system behaviour has been studied in straight track. Two different control strategies have been developed, in order to recover a stability condi-

tion.

In this thesis, linear optimal control is used for both the control strategies. This kind of feedback control has been studied and used in various applications, such as the lateral and the vertical dynamic control of the railway vehicle ([5]). The same could be said for the state estimation, in particular the Kalman filter practical application: it has been included in several situations, where a restricted set of parameters are measured, and sensors and process noises are taken into account; an example could be found in [9]. Historically, active suspensions appear in the first part of the 20th century as research and development work on various automotive vehicles. Active control on railway vehicles was introduced mainly to operate on the same infrastructure of other trains. For example, *Pendolino* train was able to operate at curving speed around 15% higher than conventional trains. This improvement is obtained by the active tilting of the carbody, that allows to reduce the non compensated trasversal acceleration due to the cant deficiency. Therefore, in railway tracks rich in tight curves as for the Italian tracks, this system permits to increase the average trip velocity, and then to reduce the travelling time ([7])

A practical application of the Secondary Yaw Control can be found in [2], where line tests with a high speed vehicle have been performed. This study is probably the closest application of Secondary yaw control that this thesis proposes to do. Other research informations on Secondary yaw control can be found in [6].

1.2   Thesis structure

The thesis is structured in the following parts:

- in Chapter 2 the mathematical model of the railway vehicle taken into account will be presented; the equations of motion and the related state space model will be computed. Moreover, a stability overview will be

assessed.

- in Chapter 3 the LQ optimal control will be studied and applied on the linear model; the choice of the regulator weights will be discussed and a result comparison with the passive model will be performed.

- in Chapter 4 the LQG control and the Kalman filter design will be presented. Considerations on the sensors will be done, and a comparison between the passive model and the two control strategies will be displayed.

- in Chapter 5 a multi body non linear simulator is taken into account, and the railway vehicle will be simulated in this environment. Several comparisons with the previous simulations will be done, and the final aim of the thesis will be assessed.

- in Chapter 6 the entire work will be summarized and will be presented the possible developments, in term of control strategy design and simulation/validation methods.

- in Appendix A the physical parameters of the linear mechanical model will be listed.

Chapter 2

Mathematical model for straight track

2.1 System description

A typical modern-style vehicle is taken into account in order to study the dynamic response and then develop the control strategies. This kind of model has got several peculiarities that could be summarized in three aspects: linear, half vehicle, plan view. Generally, a mathematical model is focused on describing reasonably the reality, and at the same time to be simple enough to permit a proper control strategy development. Physically, the model is composed by four rigid bodies: two wheelsets, a bogie and half carbody, interconnected by dampers and springs. The mechanical arrangement is shown in fig. 3.2.

Below the major assumptions are pointed out, explaining how they have been addressed.

2.1.1 Linear model

The dynamic behaviour of a railway vehicle, in general, shows different types of non-linearities; one of these is the wheel-rail contact. As explained by various authors ([1]), this mechanism is described by the creep forces (also
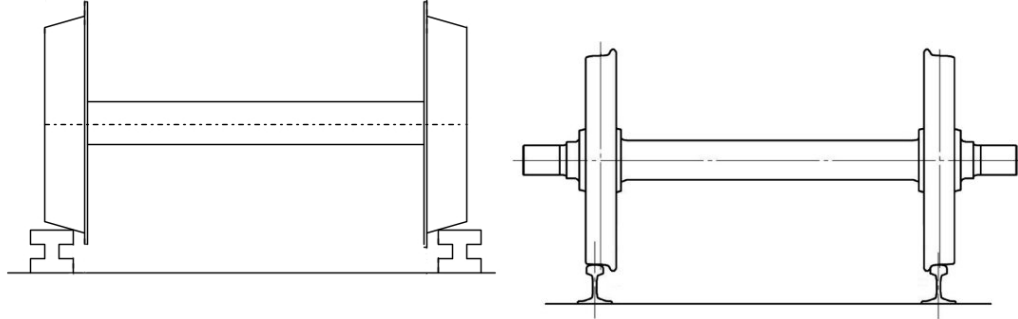
Figure 2.1: Linear conicity and non linear conicity examples

called "creepages") combined with the conicity of the wheels. Since these forces depend on the elastic deformation of the material, and the real profile of the wheel is far from a simple conicity coefficient, the modellization here is simplified trough the Kalker formulas. These formulas describe linear relationships, that are functional to a simpler control strategy development. Other causes of non-linearity may be detected, but are less incisive with respect to the contact mechanism; eventually, the advantages of including at this stage non linearities are very limited.

2.1.2 Half vehicle plan view

An half vehicle instead of a full vehicle model is taken into account because the dynamic coupling between the two bogies through the secondary suspention is small. This work is focused on the stabilization of a bogie, and the aim is to counteract the hunting instability of this element; this kind of instability affects mainly the lateral and yaw modes, therefore only a plan view model is needed. Futhermore, this choice is justified also from the fact that the plan dynamics is widely incorrelated from the vertical dynamics.

Figure 2.2: Mechanical model

2.2   Dynamic modelling

The equations describing the plan view dynamic behaviour of the railway vehicle are developed from the application of Newton's laws of motion to the individual masses and wheelsests, and the overall equations of motion for the half body vehicle shown in fig.3.2 travelling on the straight track can be derived as follows:

$$m_w\ddot{y}_f = (f_{y1} - f_{y1b} - \frac{2f_{22}}{v} - \frac{2f_{22}\lambda r_0}{lv})\dot{y}_f + (k_{y1} - k_{y1b} - \frac{W\lambda}{l})y_f$$
$$+ (\frac{2f_{23}}{v} + f_{y1b}D)\dot{\psi}_f + (2f_{22} + k_{y1b}D)\psi_f + (f_{y1} + f_{y1b})\dot{y}_b$$
$$+ (k_{y1} + k_{y1b})y_b + (Lf_{y1} - f_{y1b}(D-L))\dot{\psi}_b + (Lk_{y1} - k_{y1b}(D-L))\psi_b$$

$$I_w\ddot{\psi}_f = (Df_{y1b} + \frac{2f_{23}}{v} - \frac{I_{wy}\lambda v}{lr_0} + \frac{2f_{23}\lambda r_0}{lv})\dot{y}_f + (Dk_{y1b} - \frac{2f_{11}l\lambda}{r_0})y_f$$
$$+ (-h_{ws}{}^2(f_{x1} + f_{x1b}) - D^2f_{y1b} - \frac{2f_{33}}{v} - \frac{2f_{11}l^2}{v})\dot{\psi}_f$$
$$+ (-k_{y1b}D^2 + (-k_{x1} - k_{x1b})h_{ws}{}^2 - 2f_{23} + Wl\lambda)\psi_f$$
$$+ (-Df_{y1b})\dot{y}_b + (-Dk_{y1b})y_b + ((f_{x1} + f_{x1b})h_{ws}{}^2 + Df_{y1b}(D-L))\dot{\psi}_b$$
$$+ ((k_{x1} + k_{x1b})h_{ws}{}^2 + Dk_{y1b}(D-L))\psi_b$$

$$m_w\ddot{y}_r = (f_{y1} - f_{y1b} - \frac{2f_{22}}{v} - \frac{2f_{22}\lambda r_0}{lv})\dot{y}_r + (k_{y1} - k_{y1b} - \frac{W\lambda}{l})y_r$$
$$+ (\frac{2f_{23}}{v} + f_{y1b}D)\dot{\psi}_r + (2f_{22} + k_{y1b}D)\psi_r + (f_{y1} + f_{y1b})\dot{y}_b$$
$$+ (k_{y1} + k_{y1b})y_b + (-Lf_{y1} - f_{y1b}(D-L))\dot{\psi}_b + (-Lk_{y1} - k_{y1b}(D-L))\psi_b$$

$$I_w\ddot{\psi}_r = (-Df_{y1b} + \frac{2f_{23}}{v} - \frac{I_{wy}\lambda v}{lr_0} + \frac{2f_{23}\lambda r_0}{lv})\dot{y}_r + (Dk_{y1b} - \frac{2f_{11}l\lambda}{r_0})y_r$$
$$+ (-h_{ws}{}^2(f_{x1} + f_{x1b}) - D^2f_{y1b} - \frac{2f_{33}}{v} - \frac{2f_{11}l^2}{v})\dot{\psi}_r$$
$$+ (-k_{y1b}D^2 + (-k_{x1} - k_{x1b})h_{ws}{}^2 - 2f_{23} + Wl\lambda)\psi_r$$
$$+ (Df_{y1b})\dot{y}_b + (Dk_{y1b})y_b + ((f_{x1} + f_{x1b})h_{ws}{}^2 + Df_{y1b}(D-L))\dot{\psi}_b$$
$$+ ((k_{x1} + k_{x1b}) + h_{ws}{}^2 - Dk_{y1b}(D-L))\psi_b$$

$$m_b\ddot{y}_b = (f_{y1} + f_{y1b})\dot{y}_f + (k_{y1} + k_{y1b})y_f + (-Df_{y1b})\dot{\psi}_f + (-k_{y1b})\psi_f + (f_{y1} + f_{y1b})\dot{y}_r$$
$$+ (k_{y1} + k_{y1b})y_r + (-Df_{y1b})\dot{\psi}_r + (-k_{y1b})\psi_r + (-2f_{y1} - f_{y2} - 2f_{y1b})\dot{y}_b$$
$$+ (-2k_{y1} - k_{y2} - 2k_{y1b})y_b + f_{y2}\dot{y}_v + k_{y2}y_v$$

$$
\begin{aligned}
I_b \ddot{\psi}_b =& (Lf_{y1} - Df_{y1b} - f_{y1b}(D-L))\dot{y}_f + (Lk_{y1} - Dk_{y1b} - k_{y1b}(D-L))y_f \\
& + (h_{ws}{}^2(f_{x1} + f_{x1b}) + D^2 f_{y1b} + Df_{y1b}(D-L))\dot{\psi}_f \\
& + (h_{ws}{}^2(k_{x1} + k_{x1b}) + D^2 k_{y1b} + Dk_{y1b}(D-L))\psi_f \\
& + (Df_{y1b} - Lf_{y1} + f_{y1b}(D-L))\dot{y}_r + (Dk_{y1b} - Lk_{y1} + k_{y1b}(D-L))y_r \\
& + (h_{ws}{}^2(f_{x1} + f_{x1b}) + D^2 f_{y1b} + Df_{y1b}(D-L))\dot{\psi}_r \\
& + (h_{ws}{}^2(k_{x1} + k_{x1b}) + D^2 k_{y1b} + Dk_{y1b}(D-L))\psi_r \\
& + (-2h_{ws}{}^2(f_{x1} + f_{x1b}) - A_d{}^2 f_{x2} - 2L^2 f_{y1} - 2f_{y1b}(D-L)^2 - 2Df_{y1b}(D-L))\dot{\psi}_b \\
& + (-2h_{ws}{}^2(k_{x1} + k_{x1b}) - k_{\psi2} - 2L^2 k_{y1} - 2k_{y1b}(D-L)^2 - 2Dk_{y1b}(D-L))\psi_b
\end{aligned}
$$

$$
m_v \ddot{y}_v = f_{y2}(\dot{y}_b - \dot{y}_v) + k_{y2}(y_b - y_v)
$$

(2.1)

where y_f and y_r are respectively the lateral displacements of the front and rear wheelsets, ψ_f and ψ_f are the yaw angles of the front and the rear wheelsets, y_b and y_v are the lateral displacements of the bogie and the vehicle body, and ψ_b is the yaw angle of the bogie. The vehicle model parameters used in Equation 2.1 are explained by Figure 3.2. The numerical values taken into account in the simulations are listed in Appendix A, "Sybols and parameters values". From the previous equations of motion, a state space form can be derived in order to study a model based control. As described in [4], the mathematical model is then written as:

$$
\begin{cases}
\dot{x} = Ax + Bu \\
y = Cx + Du
\end{cases}
$$

(2.2)

where

$$
x = [\dot{y}_f \ \dot{\psi}_f \ \dot{y}_r \ \dot{\psi}_r \ \dot{y}_b \ \dot{\psi}_b \ \dot{y}_v \ y_f \ \psi_f \ y_r \ \psi_r \ y_b \ \psi_b \ y_v]^T
$$

(2.3)

is the state vector. The first equation of 2.2 describes the states of the dynamic model, listed in equation 2.3. Matrix A, as explained in [4], can be derived from the motion equations, and it contains crucial informations on

the stability of the system. At this stage, B matrix, that defines the inputs that affect the system, is not present; afterwards, when a control action will be defined, B matrix will be added to the model.

The second equation of 2.2 describes the measurements performed on the system; these are defined by the sensors mounted on the train. In particular, C matrix concerns the sensors arrangement; this part will be explained better in Chapter 4, "Sensing assessment". Matrix D, as for matrix B, is not present because there is not direct transfer between inputs and measurements.

2.3 Track characteristics

As it can be noticed, the previous model hasn't got any exogenous input; a typical exogenous source in this case could be a lateral track irregularity. In order to perform this addition, a modification must be done in the state space model definition. The first equation of 2.2 becomes:

$$\dot{x} = Ax + Bu + Ed$$

where E matrix defines the transfer between the disturbancies and the states. Consequently, also the outputs equation changes, getting a new term Fd:

$$y = Cx + Du + Fd$$

Matrix F, as already said for matrix C, will be treated in Chapter 4. Therefore, two different track irregularities have been included in order to test the response of the mathematical model. These strategies have been used with two different purposes: to understand how qualitatively is the response of the system, in order to recover the passive performances, and then to see the performances in a realistic scenario. The aim of the thesis, specifically the desired better curving performance, at this stage cannot be evaluated; this is because of the straight structure of the track. Afterwards, with the non linear multi body model (Chapter 5), the performances of all the configura-
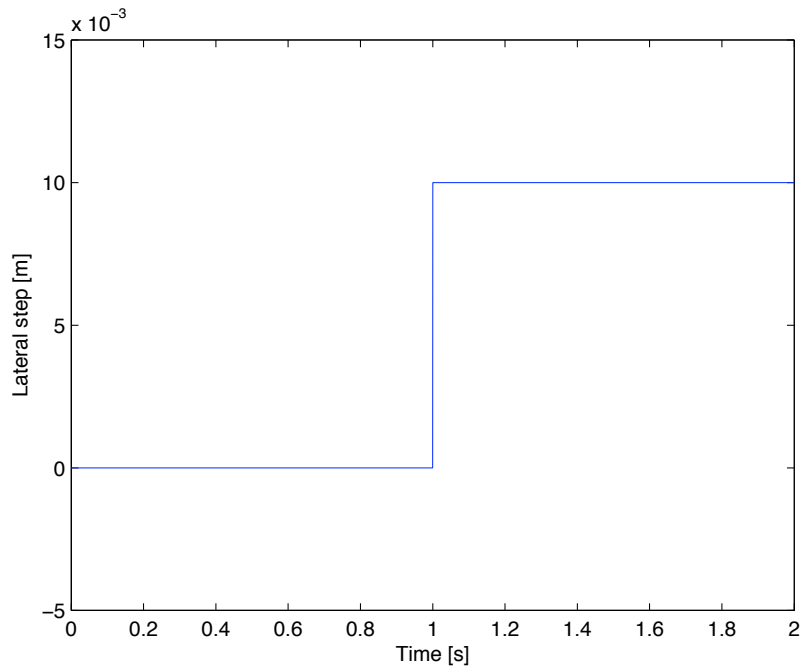
Figure 2.3: Example of lateral step disturbance, 0.01 m

tions will be studied.

Below a detailed analysis of the two straight track strategies is presented.

2.3.1   Lateral step

Firstly, a deterministic input has been considered. A step profile has been chosen in order to assess the stability and the damping performances on each degree of freedom. In a first approximation, this kind of input may be assumed as a isolated lateral disturbance, that affects the system at a certain point and leaves it to reach the steady state condition. A simple lateral step is particularly useful because it makes the comparison between two different configurations very simple and straightforward. A typical example is shown in fig. 2.3, where the amplitude of the lateral displacement is 0.01 m.
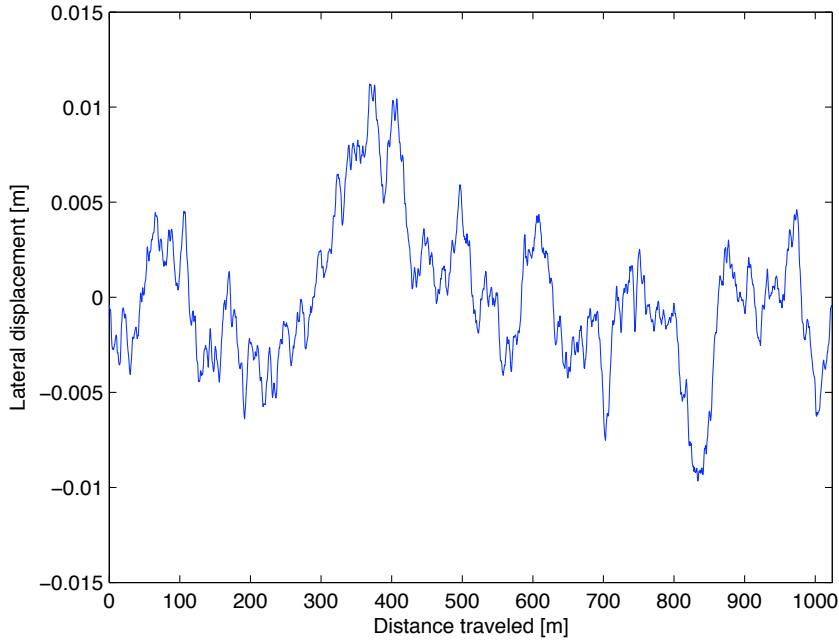
Figure 2.4: Example of lateral measured disturbance

2.3.2 Real disturbance

Track irregularity measurements are available from track recording vehicles for different route situations; a representative extract has been chosen and used for the simulations (figure 2.4). Here the purpose is to test firstly the passive system, and then to compare these results with the two control strategies. This kind of simulation is useful because, taking into account the measurements obtained from the sensors, it permits to evaluate the dynamic performances in a realistic situation, recovering the passive performances with the active control strategies.

2.4 Eigenvalues and stability analysis

Based on the derived plan view half vehicle dynamic model, an eigenvalue analysis is performed so as to determine the natural frequencies of the vehicle

dynamic modes and the damping ratios associated with each mode; the results are shown in table 2.1. The analysis has been performed with the numerical values listed in Appendix A. It can be seen that a few kinematic modes are shown; these are the ones that display a frequency below 10 Hz and a damping ratio lower than 1. In order to evaluate the stability of the system, these two parameters are taken into account: in particular, when a damping ratio becomes negative, this is related to an unstable mode. In other words, this means that the associated eigenvalue has reached positive real part.

In the model that has been taken into account several parameters affect the running performances and the resulting stability. The most important are two: λ, linear conicity coefficient and v, vehicle forward velocity. As a first analysis, it can be said that velocity and conicity are inversely proportional to the stability: the more these values increase, the less the vehicle is stable. In fact, as it can be seen in the equations of motion, when they become larger, they both concur to decrease the damping contribution in the lateral and yaw dynamics of the wheelsets. In general, the damping contribution helps to dissipate the energy of the system. When this value becomes lower, and in the worst case negative, this means that the system is not dissipating all the energy that is gaining, and when it is negative it is feeding the instability phenomenon. This is why hunting instability occours: a linear model shows that conicity and velocity are closely related to this issue.

In practice, using the lateral step input, several simulations have been performed in order to test the dynamic response of the system.

Frequency (Hz)	Damping ratio
65.5045	1.0000
64.6107	1.0000
52.5615	1.0000
54.6719	1.0000
24.4032	0.6401
10.4439	0.1924
6.6219	0.9107
3.0066	0.1771
0.6813	0.2207

Table 2.1: Eigenvalue analysis

2.5   Primary yaw stiffness analysis

As already explained in the introduction, primary yaw stiffness plays a pivotal role in railway vehicle mechanical design. Basically, when a bogie is designed, a proper primary yaw stiffness value has to be chosen in order to ensure adequate curving performance, and at the same time providing stability, primarily in straight track.

Another parameter, concerning to the stability problem, could be then considered the value of primary yaw stiffness of the single wheelset.

As it can be easily understood, a lower value of primary yaw stiffness makes the model less stable; intuitively, hunting instability will then occour at a lower velocity. On the other hand, if an active control can give stability to the system, curving performances will take advantage; therefore, it must be found the right reduction of primary yaw stiffness. The final target can be considered the achievement of 10% of the original primary yaw stiffness. Hereinafter, all the control strategy design are based on this target.

In Figures 2.5, 2.6 and 2.7, a brief explaining of the passive system perform-
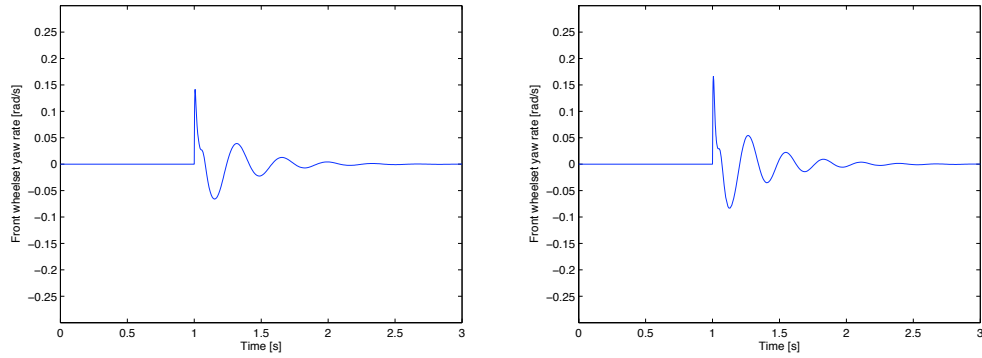
Figure 2.5: $v = 40$ *m/s and* $v = 50$ *m/s,* λ=0.15, p.y.s.=100%
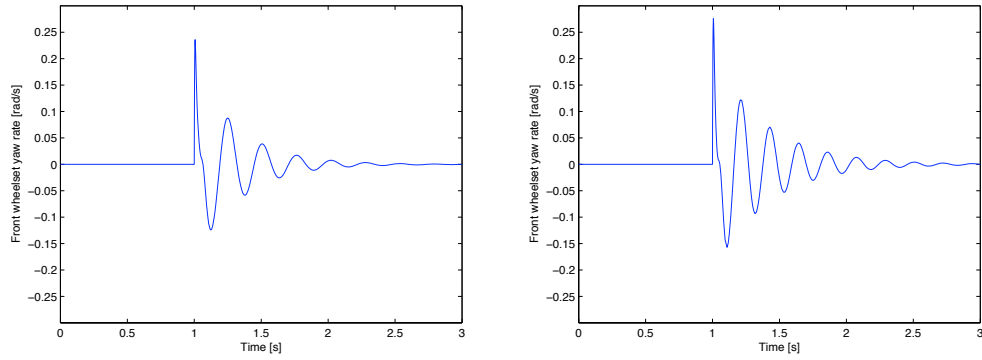
Figure 2.6: $v = 40$ *m/s and* $v = 50$ *m/s,* λ=0.25, p.y.s.=100%

ances is proposed. The results are displayed in two different ways: a time history and a eigenvalue plot. The time history is referred to a single degree of freedom, specifically the yaw rate of the front wheelset, $v = 40$m/s, forced with a step input, 0.01 m of amplitude; concerning to the eigenvalues, a negative damping means an unstable mode.
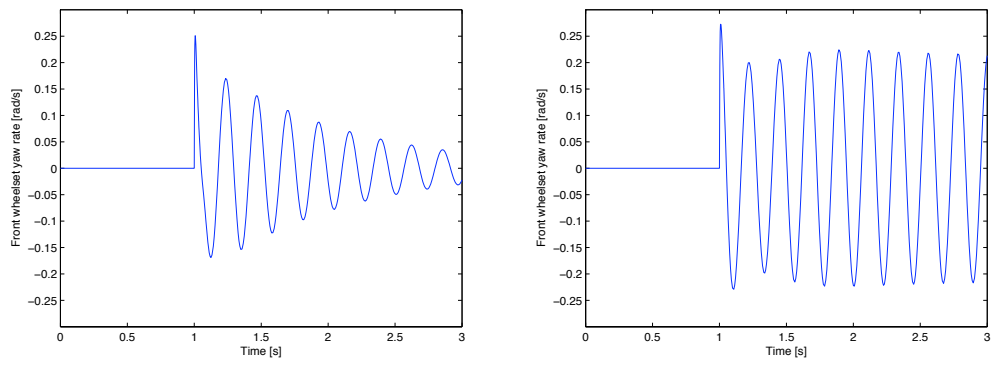
Figure 2.7: $v = 40$ *m/s*, λ=0.25, *p.y.s.=50% and p.y.s.=10%*

Chapter 3

LQR control

3.1 Introduction

In this chapter an application of a full state optimal control is presented. Firstly, the linear quadratic optimal control theory is discussed, and then it is implemented in this case, as explained in Chapter 1, "Introduction".

Optimal control has been applied in various fields of automotive problems, such as active suspensions in automobiles, but also in the railway branch. Here, this kind of control is taken into account in order to overcome the trade-off between stability and curving performances, as discussed before. Below the first optimal control strategy is presented, an LQ full state regulator; afterwards another control strategy will be presented, an LQG control with state estimation. These two strategies could be considered as classical approaches of optimal control: these have been taken into account as logical beginning of a state-based control. Possible developments in this field will be discussed in Chapter 6, "Conclusions".

3.1.1 Linear Quadratic optimal control (LQ)

The control method, as generally for optimal control, is obtained from an appropriate problem of optimization in time domain. In this way, in the formulation of the control it is possible to include potential constraints on

the state and control variables; these are defined by the weights that can be found in the cost function. LQ control deals with linear quadratic cost functions.

Considering a linear, time invariant system where the state is accessible,

$$\dot{x}(t) = Ax(t) + Bu(t)$$

is the state equation. Concerning to the figure of merit,

$$J(x_0, u, 0) = \int_0^{+\infty} (x'(\tau)Qx(\tau) + u'(\tau)Ru(\tau))d\tau \qquad (3.1)$$

is the linear quadratic formula, where

$$Q = Q' \geq 0, \ R = R' > 0$$

are design parameters. Q and R matrix are almost always diagonal, but there is no specific form restriction. Taking into account the Riccati differential equation,

$$\dot{P} = A'P + PA + Q - PBR^{-1}B'P = 0 \qquad (3.2)$$

and the associated linear control law,

$$u = -R^{-1}B'Px = -K_r x$$

subject to (A, B) controllable, (A, C_q) observable, and Q is constructed as $Q = C_q'C_q$. K_r is the matrix that minimises the cost function written in 3.1. In 3.2, $\dot{P}$ has been set to zero because the optimization problem is considered on a infinite horizon. This control law is time-invariant and it does not need the knowledge of the current state; therefore, it can be computed a priori.

3.1.2 LQR tuning

The optimization of the figure of merit is made through the state weighting matrix Q and the control weighting matrix R, that allow to weight the single state and the control action, respectively. It is interesting to note that the weighting on the states is positive semi-definite, that is sensible: a single

state is weighted as required, and at limit it is set to zero. Hence negative weighting does not make sense. Differently, the weighting on the control is only positive definite: this is due to the fact that a weight on the control is necessary to ensure that the state is not set to zero instantaneously with a very high control.

Since in some difficult cases it could be hard to tune Q and R matrices, for example where the number of states is high, several methods have been developed in order to select these matrices in a simple way.

One of these is the states and control normalization. Setting as

$$Q = \begin{bmatrix} q_1 & 0 & 0 \\ 0 & \ddots & 0 \\ 0 & 0 & q_s \end{bmatrix}, \; q_i \geq 0; \quad R = \begin{bmatrix} r_1 & 0 & 0 \\ 0 & \ddots & 0 \\ 0 & 0 & r_c \end{bmatrix}, \; r_i > 0$$

the states and control matrices, the cost function becomes

$$J = \int_0^{+\infty} (q_1 x_1^2(\tau) + ... + q_s x_s^2(\tau) + r_1 u_1^2(\tau) + ... + r_c u_c^2(\tau))d\tau$$

Taking into account the maximum values that can be assumed by the states and the inputs, the weights may be rewritten as

$$q_i = \frac{\bar{q}_i}{x_{max}^2}, i = 1, ..., s, \quad r_i = \frac{\bar{r}_i}{u_{max}^2}, i = 1, ..., c, \quad \bar{q}_i \geq 0, \; \bar{r}_i > 0 \quad ;$$

then the cost function becomes

$$J = \int_0^{+\infty} \left(\bar{q}_1 \frac{x_1^2(\tau)}{x_{max}^2} + ... + \bar{q}_s \frac{x_s^2(\tau)}{x_{max}^2} + \bar{r}_1 \frac{u_1^2(\tau)}{u_{max}^2} + ... + \bar{r}_c \frac{u_c^2(\tau)}{u_{max}^2} \right) d\tau$$

In this way, the single state is automatically weighted on its maximum value; $\bar{q}_i$ and $\bar{r}_i$ are weighting on values included between 0 and 1. This is a good starting point in order to tune a complex system.

3.2 LQ regulator design

As presented in the previous section, in order to design a proper LQ regulator several parameters have to be defined; the target of this control design is to roughly recover the passive system performances.

Figure 3.1: Anti-yaw damper,secondary yaw control: passive and active approaches

3.2.1 Weights tuning

Since in this case the state vector contains 14 variables, the first weighting attempt is done with the state normalization. The maximum values assumed by the states have been obtaned from a number of simulations on the passive model; it is important to note that these simulations are performed on the linear system, with the original value of primary yaw stiffness. In some cases the assumption of linearity, especially for large deflection of the springs/dampers, gives results that are not reliable, because the simulation could deviate sensibly from the reality. Practically, taking into account recorded lateral track disturbancies, the maximum value of the single state has been measured, and then used in the Q matrix. Concerning to the R matrix, it has been considered the damper on the passive model, in particular the maximum force exerted by this element. Therefore, the weights associated to an angular velocity are expressed in s^2/rad^2, lateral velocity s^2/m^2, angular displacement $1/rad^2$, lateral displacement $1/m^2$, input force $1/N^2$. Below this first attempt is displayed, remembering also the state vector.

$$x = [\dot{y}_f \ \dot{\psi}_f \ \dot{y}_r \ \dot{\psi}_r \ \dot{y}_b \ \dot{\psi}_b \ \dot{y}_v \ y_f \ \psi_f \ y_r \ \psi_r \ y_b \ \psi_b \ y_v]^T \tag{3.3}$$

$$Q_n = diag[38, 1.79*10^2, 57, 1.04*10^2, 41, 1.96*10^2, 92, 1.16*10^3, 6.92*10^4, ...$$

$$...4, 96*10^3, \ \ 5.17*10^4, \ \ 4.5*10^3, \ \ 7.71*10^4, \ \ 2.83*10^3]$$

$$R = [1.29*10^{-9}]$$

Figure 3.2: Mechanical model with secondary yaw actuators

These two matrices produce a gain matrix and then a control law that is used as shown in figure 3.3. The gain matrix is then

$$K_{rn} = [-6.2*10^3 \ \ 8.3*10^3 \ \ -8.1*10^3 \ \ 2*10^3 \ \ -2.1*10^4 \ \ 1.2*10^6 \ \ 8.6*10^4...$$

$$... -2.2*10^6 \ \ 3.6*10^6 \ \ -4.1*10^6 \ \ 1.3*10^6 \ \ -8.7*10^5 \ \ 4.7*10^6 \ \ 1.2*10^5]$$

where the gains associated to an angular velocity are expressed in $kg \cdot m/rad \cdot s$, lateral velocity kg/s, angular displacement $kg \cdot m/rad \cdot s^2$, lateral displacement kg/s^2, because the resulting control law must be a linear force.

Starting from these very initial values, a more precise tuning is then performed. First of all, the maximum performances of the actuator must be taken into account. As explained in [2], a sensible value of maximum force required in a secondary yaw control architecture is around 5-8 kN; this bond results in an accurate weighting of the bogie yaw rate. Secondly, it is important to consider comfort performances for the passengers, that means to

keep under a sensible threshold the accelerations of the system. In general, large values of velocities and accelerations on the states of the model are undesired because the mechanical parts, for example spring or dampers, have got physical limits that cannot be overcome. Hence, the values assumed from the passive system are a suitable term of comparison. Below the adjusted weights in the Q matrix.

$$Q = Q_n \cdot [1 \quad 1 \quad 1 \quad 1 \quad 1 \quad 15 \quad 1 \quad 0.1 \quad 1 \quad 0.1 \quad 1 \quad 1 \quad 1 \quad 0.1]^T$$

The associated gain matrix becomes

$$K_r = K_{rn} \cdot diag[1.02, \quad 0.32, \quad 0.62, \quad 0.14, \quad 1.14, \quad 3.65, \quad 0.56, \quad ...$$

$$...0.7, \quad 0.45, \quad 0.71, \quad 0.37, \quad 0.54, \quad 0.86, \quad 0.1] \tag{3.4}$$

With this setting, the maximum force exerted by the motor is 7.6 kN, that is an acceptable value. It is interesting to notice that, both in the Q matrix and K_r array, the value associated to the bogie yaw rate differs visibly from the other values. This is due to the fact that in Q matrix the associated weight has to be high enough to not exceed the maximum force of the motor; in the gain array, it points out that the bogie yaw rate is the most important component used in the feedback. Intuitively, this is correct because in the passive situation the anti-yaw damper works only on the bogie yaw rate, therefore it is the most important component.

3.2.2 Active control actuator

At this point, it is important to show where the active control acts into the equations of the system. The yaw damper, the mechanical device that counteracts the action of hunting instability, affects the equation of momenta of the bogie. Therefore, in the active system this component must be eliminated. Active control replaces the function of this mechanical part using an electric drive. Practically, the motor must be placed in the same position of the damper, and through a transmission the rotational movement of the

motor is converted to a linear motion, as shown in figure 3.1. Here all the mechanical dynamics of the motor, for reason of simplicity, are not taken into account; the only parameter that has been considered is the maximum force that can be exerted by the motor.

Therefore, in order to include the actuator in the mathematical model, B matrix has been used to define the control input.

With these informations, a number of simulations have been performed, in order to validate the stability of the new mechanical system with the lowered primary yaw stiffness; in the next section the results will be displayed.

3.3 Linear simulation

Here some sample demonstrations of the control strategy are shown. In Figure 3.3 the simulation structure can be seen, and it is composed by:

- lateral track disturbance that acts on the front and the rear wheelsets

- state space model that describes the system

- feedback with the LQR gain array

- full state measurement

The results are displayed, in terms of time domain simulations, as a comparison of the passive and the active system, on different degrees of freedom. The aim of roughly recover the passive system performances is reached; taking into account that the primary yaw stiffness is reduced to 10% of the original value, some differences can be tolerated. A time history comparison has been chosen (i.e. instead of a root locus chart) because it better shows the differences/similarities of the two different models. The simulation characteristics are $v = 40$ m/s, $\lambda = 0.15$.
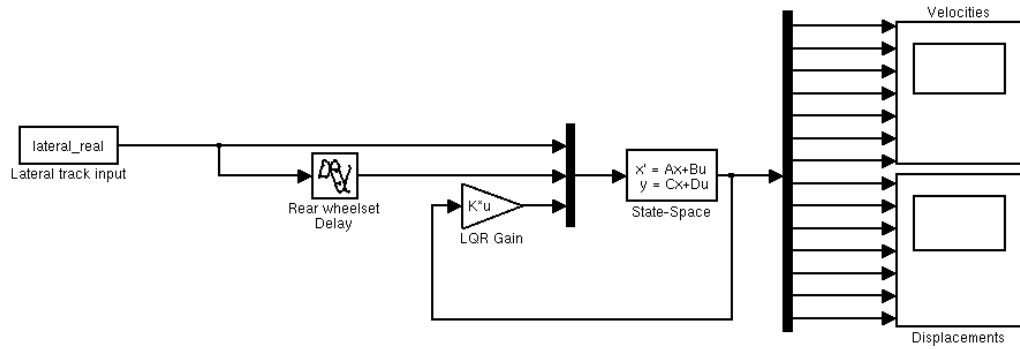
Figure 3.3: LQR simulation
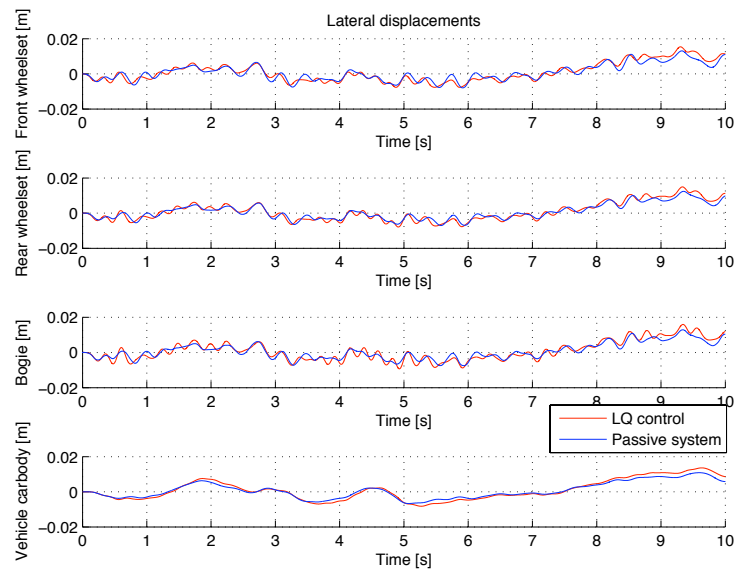

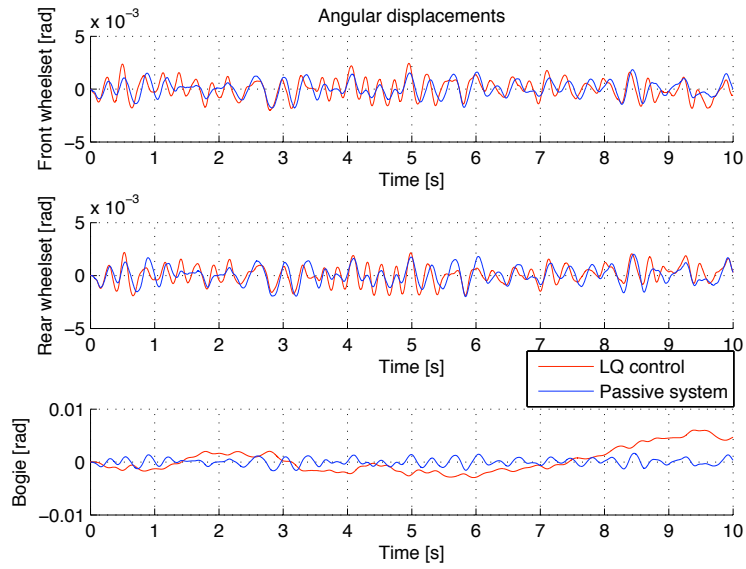Figure 3.4: Performances comparison: active and passive lateral displacements

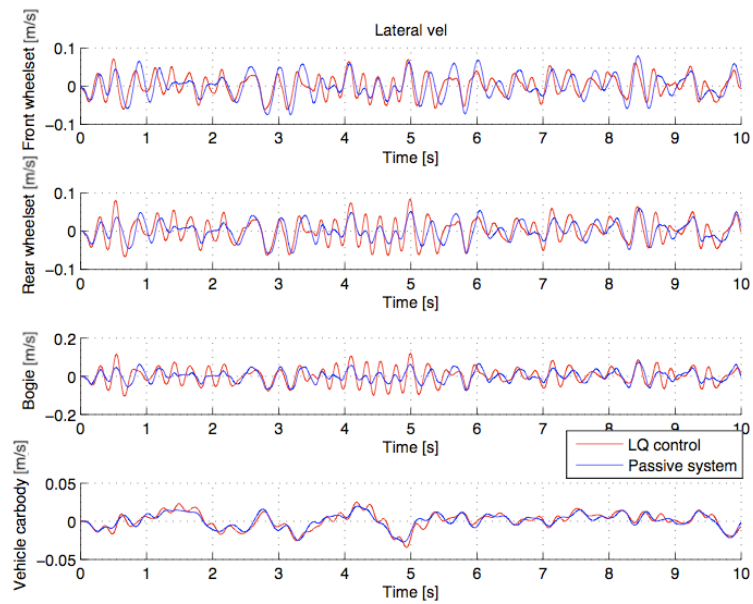*Figure 3.5: Performances comparison: active and passive angular displacements*

Figure 3.6: Performances comparison: active and passive lateral velocities
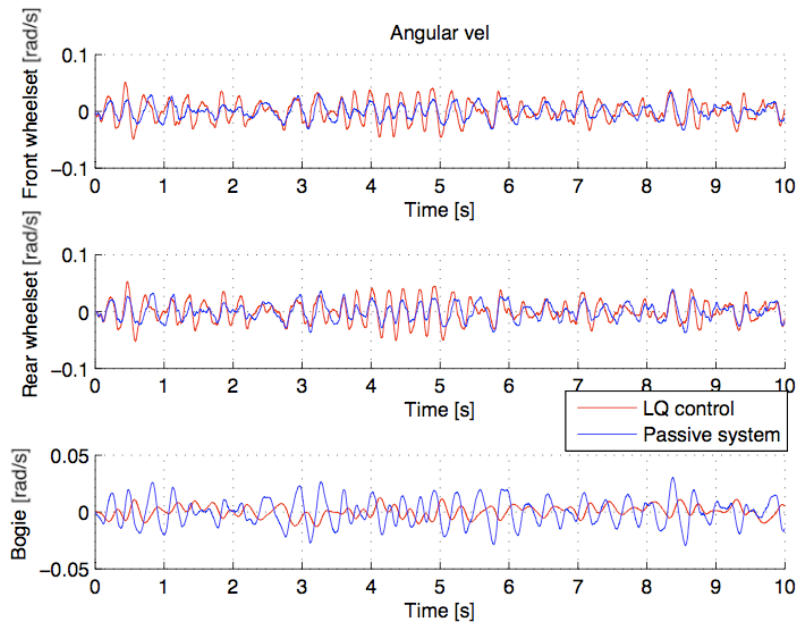
Figure 3.7: Performances comparison: active and passive angular velocities

3.4 From LQR to LQG control

Intrinsically, the structure of an LQ regulator needs the complete knowledge of the states, in order to produce a control action through the gain matrix. This is a very restrictive assumption, because in the real world it is very difficult to measure all the states. Measurements need sensors, that have to be placed on the mechanical system. These two statements highlight several problems: some sensors could have an undesiderable high cost, and it is not always possible to place a certain sensor on the system. Moreover, sometimes some states are physically unmeasurable.

Therefore, starting from a restricted set of measurement it is necessary to estimate the entire state of the system. This is why, in the next chapter, the development of a state estimator is discussed and then applied in a control strategy. In this case, an appropriate state estimator is the Kalman filter, because it fits fairly well the problem that is considered in this study.

At this point, it is important to underline that an LQR control can not be

a realistic solution of the problem, especially in this case, where a railway vehicle is taken into account. However this control strategy has been developed because it constitutes the natural first step for an optimal control, and above all it is a term of comparison for the control with state estimation.

Chapter 4

LQG control with sensing assessment

4.1 Introduction

As explained in the previous chapter, a Linear Quadratic Gaussian control has been developed. In this chapter the structure of this control strategy is firstly shown, and then implemented on the system. LQG control is obtained from an LQ control law in combination with a Kalman filter, that is used to get the estimation of the states where the system is affected by stochastic disturbances.

This kind of control strategy could be considered as an evolution compared to the LQ approach, because it takes into account more realistically the circumstances in which the system is inserted. In order to produce an LQ regulator, a full knowledge of the states is needed; this assumption is particularly strong where the system owns a considerable number of degrees of freedom. Moreover, measurements are inevitably affected by noise and errors, that must be taken into account; the system can be also affected by disturbances. LQG control takes into account the issues listed above, because the purpose of the Kalman filter is precisely to estimate the entire state of the system with a restricted set of measurements affected by noise. It is important to

note that the control is called "Gaussian": the model disturbances and the measurement noises must be modeled as Gaussian white noises.

4.1.1 Kalman filter

The Kalman filter is a state obsever with optimality peculiarities, that must be implemented when the system is affected by stochastic disturbances. Considering the linear system

$$\begin{cases} \dot{x} = Ax + Bu + v_x \\ y = Cx + v_y \end{cases} \tag{4.1}$$

where v_x is the process noise and v_y is the measurements noise; these are uncorrelated gaussian white noises with zero mean, and covariance matrix V defined as

$$v = \begin{bmatrix} v_x \\ v_y \end{bmatrix}, \quad E[v(t)] = 0, \quad E[v(t_1)v(t_2)'] = V\delta(t_1 - t_2)$$

$$V = \begin{bmatrix} \tilde{Q} & 0 \\ 0 & \tilde{R} \end{bmatrix}$$

where δ is the Kroenecker index. Noises on the states and on the output are assumed to be uncorrelated.

Therefore, the observer taken into account is

$$\dot{\hat{x}}(t) = A\hat{x}(t) + Bu(t) + L(t)[y(t) - C\hat{x}(t)]$$

where $L(t)$ is a time variant gain chosen to meet an optimality criterion. As already explained for the LQ control, a time invariant law can be produced:

$$\dot{\hat{x}}(t) = A\hat{x}(t) + Bu(t) + \overline{L}[y(t) - \hat{y}(t)] = A\hat{x}(t) + Bu(t) + \overline{L}[y(t) - C\hat{x}(t)] =$$

$$= (A - \overline{L}C)\hat{x}(t) + Bu(t) + \overline{L}y(t) \tag{4.2}$$

where

$$\overline{L} = \overline{\overline{P}}C'\tilde{R}^{-1}$$

35

with $\overline{\tilde{P}}$ is the unique definite positive solution of the Riccati equation

$$0 = A'\overline{\tilde{P}} + \overline{\tilde{P}}A + \tilde{Q} - \overline{\tilde{P}}C'\tilde{R}^{-1}C\overline{\tilde{P}} \tag{4.3}$$

This result is subjected to (C, A) observable, $\tilde{Q} \geq 0$, and (A, B_q) controllable, where $Q = B_q B_q'$. The estimator thus obtained is asimptotically stable, because the eigenvalues of $(A - \overline{L}C)$ have negative real part.

4.1.2 Linear Quadratic Gaussian control (LQG)

The structure of the LQG control is obtained combining an LQ control law and a Kalman filter in order to reconstruct the state of the system affected by stochasthic disturbances. Similarly to the LQ control, the LQG control law is obtained through an optimization in the time domain, with some modifications. Below, the mathematical theory of the control is presented. Taking into account the same system of the Kalman filter (Equations 4.1), the figure of merit considered is

$$J = \lim_{T \to \infty} \frac{1}{T}E\left[\int_0^{+\infty}(x'(t)Qx(t) + u'(t)Ru(t))dt\right] \tag{4.4}$$

where x is non measurable. Through several mathematical steps, it is possible to reach the final formulation:

$$J = E\left[x'(t)Qx(t) + u'(t)Ru(t)\right] \tag{4.5}$$

Therefore, it is possible to use the same control law used in the LQ control, combining the Kalman filter and LQ control hypotesis explained previously:

$$u(t) = -\overline{K_r}\hat{x}(t)$$

$\overline{K_r}$ is obtained from the estimation made by the Kalman filter; the $\overline{L}$ optimal gain and then the state estimation is made ignoring the fact that the system is fed back. Basically, it is assumed that the control scheme and the state estimation operate separately. Eventually, it is possible to demonstrate that the closed loop eigenvalues are the combination of the two components: $(A - \overline{L}C)$ and $(A - B\overline{K})$.
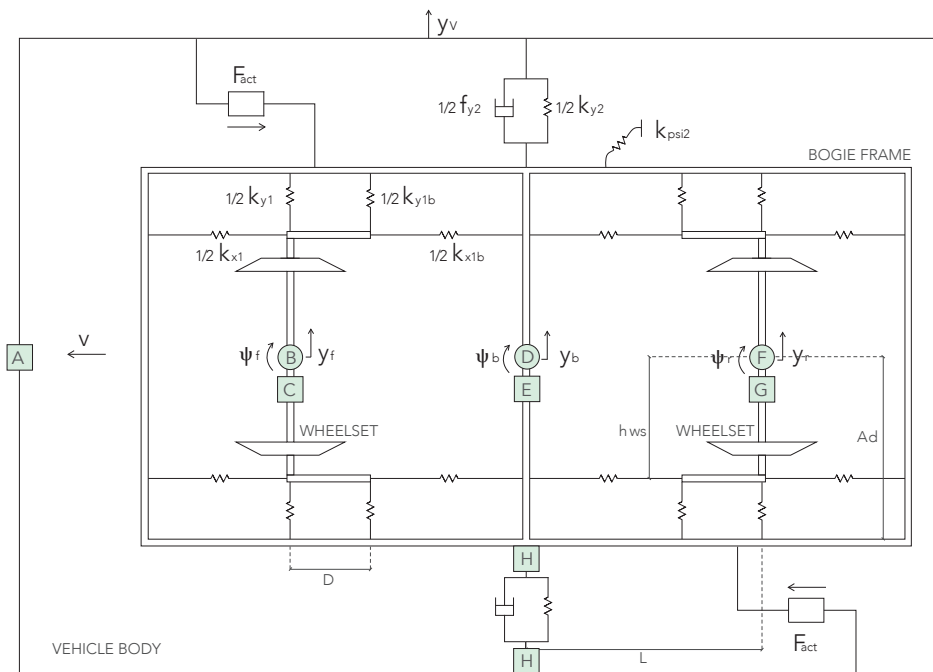
Figure 4.1: Sensors configuration on the considered vehicle

4.2 Sensing assessment

The main difference between LQ and LQG approach, as already explained, consists in considering the real measurements performed on the mechanical system. As it can be easily understood, different numbers and types of sensors affect the characteristics of the measurements, therefore they affect the results of the state estimation.

In this work has been taken into account a realistic configuration: below, the sensors mounted on the simulated vehicle are listed.

Letter	Measure	Sensor
A	$\ddot{y}_v$	Carbody lateral accelerometer
H	$y_v - y_b$	Relative distance between bogie and carbody
E	$\dot{y}_b$	Bogie lateral accelerometer
D	$\dot{\psi}_b$	Bogie yaw rate (gyroscope)
C,G	$\ddot{y}_f, \ddot{y}_r$	Front and rear wheelset lateral accelerometer
B,F	$\dot{\psi}_f, \dot{\psi}_r$	Front and rear wheelset yaw rate (gyroscope)

Table 4.1: List of sensors

Starting from these measurements, it is possible to reconstruct the full state of the system. Theoretically, this could be done through a simple derivation/integration of the measured signals, listed in Table 4.1. In practice, this method is rarely used because the direct integration or derivation of the signal leads to unreliable and very often incorrect results. For example, a typical cause of error is the integration drift produced by low frequency components in a signal.

Here it is used a continuos Kalman filter, as explained in Section 4.1, that reconstructs the state used to produce the LQ regulator gain.

In order to introduce the sensors in the mathematical model, a number of modifications have been done, in particular in C and F matrix. In LQ control, the output equation of the state space model has been set to display all the states. Differently, in this case C matrix has to be set to display the signals measured by the sensors; F matrix contains the disturbances transferred on the measurements. Here the matrices are defined with subscript $_s$ to indicate the difference from the LQ matrices.
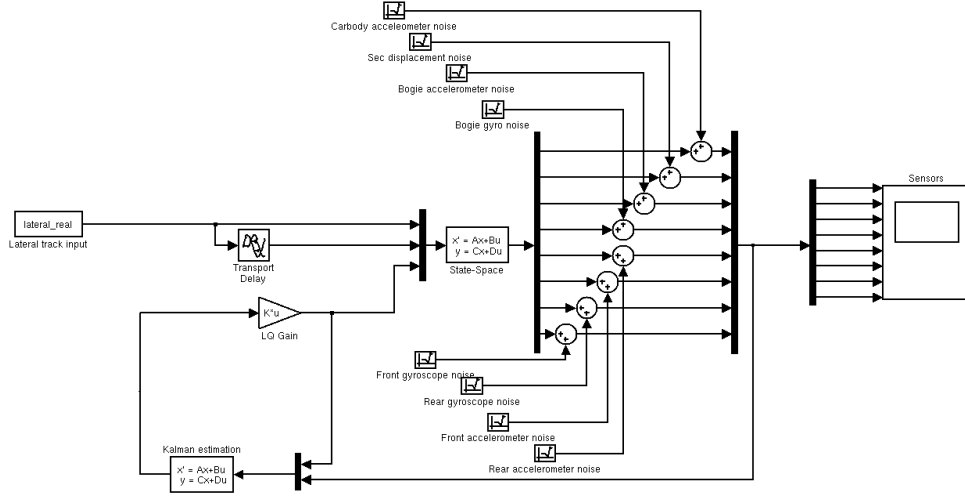
$$
C_s = \begin{bmatrix}
A(7,\cdot) \\
0\ 0\ 0\ 0\ 0\ 0\ 0\ 0\ 0\ 0\ 0\ 1\ 0\ -1 \\
A(5,\cdot) \\
0\ 0\ 0\ 0\ 0\ 1\ 0\ 0\ 0\ 0\ 0\ 0\ 0\ 0 \\
A(1,\cdot) \\
A(3,\cdot) \\
0\ 1\ 0\ 0\ 0\ 0\ 0\ 0\ 0\ 0\ 0\ 0\ 0\ 0 \\
0\ 0\ 0\ 1\ 0\ 0\ 0\ 0\ 0\ 0\ 0\ 0\ 0\ 0
\end{bmatrix}
, \quad
F_s = \begin{bmatrix}
0\ 0 \\
0\ 0 \\
0\ 0 \\
0\ 0 \\
E(1,\cdot) \\
E(3,\cdot) \\
0\ 0 \\
0\ 0
\end{bmatrix}
$$

As it can be seen, both matrices contain an entire row of the A or E matrices. This is due to the fact that an acceleration is obtained from a velocity state equation, that has been taken from the left part of the expression $(\dot{x}_v = \dots)$ and put in the right part $(\cdots = \dot{x}_v)$. In this way, the output equation describes the derivative of the velocity, that is exactly the desired acceleration $(y = \dot{x}_v)$. The other rows are composed by zeros and ones, that represent the pure states set as outputs.

Every single sensor has got its own characteristics, defined in the corresponding data sheet. An important information is the noise introduced by the sensor, because it means that the measure does not represent exactly the reality. As expressed in Equation 4.1, the Kalman filter has been designed to take into account this problem, in the particular case of Gaussian-distributed noises. In Section 4.3 noise modellization is discussed for each sensor.

Figure 4.2: Simulink model of LQG control

4.3 LQG control design

Similarly to what has been presented in Chapter 3, also for LQG control several parameters have to be chosen; in addition, the Kalman filter tuning has to be decided. Here the target is to achieve the same performances of the LQ control, but including the step of the state estimation.

The complete state space model, including the lateral track disturbances, the control action and the measurement noise become

$$\begin{cases} \dot{x} = Ax + Bu + Ed \\ y = C_s x + F_s d + v_y \end{cases} \tag{4.6}$$

Considering this model structure, it is possible to discuss the final configuration of the control.

4.3.1 LQ weights and Kalman filter tuning

Concerning to the LQ regulator design, it has been used the same tuning and therefore the same K_r gain array, written in Equation 3.4.

In order to design a proper state estimation, the model form written in Equation 4.6 is considered; therefore, the proper MATLAB function has

40

been chosen. The function that fits the considered problem is *lqew*, because it is based exacly on the state space written in Equation 4.6. This function needs specific inputs, that are basically the informations needed by a Kalman filter built on these equations. $E[\gamma]$ is intended to be the expected value of γ, differently from E, disturbancies matrix on the state equation.

Below, the input information needed for the state estimation are listed:

- $E[dd'] = Q$, lateral disturbancies covariance

- $E[vv'] = R$, sensors noise covariance

- A, C_s, E, F_s, matrices of the state space model

From this information, the Kalman filter gain $\overline{L}$ is computed, and then the full state is reconstructed.

$$\dot{\hat{x}} = A\hat{x}(t) + Bu(t) + \overline{L}[y - C\hat{x}]$$

The Q matrix has been simply calculed as the variance of the lateral disturbancies signal used in the simulation. The result, used in the simulation, is $1.4235 * 10^{-5} m^2$. Of course, this value depends on the characteristichs of the disturbance: since a limited examples of disturbancies have been used, the variance is calculated a priori, and then put in the simulation. In order to avoid this limitation, it could be done a variance average on several files of lateral disturbancies, in order to reach a reliable and general value.

As regards the R matrix, it has to be taken into account the noise of the single sensor. Practically, as it can be seen in Figure 4.2, a Gaussian white noise has been added to the measure, with a precise value of variance. This value has been assumed to be the 1% of the full scale of the sensor. Below, the variances of each sensor are listed:

- wheelset lateral accelerometer: $3.6 * 10^{-3} m^2/s^4$

- bogie lateral accelerometer: $2.5 * 10^{-3} m^2/s^4$

- carbody lateral accelerometer: $1.6 * 10^{-3} m^2/s^4$

- wheelset yaw rate gyroscope: $2.89 * 10^{-6} rad^2/s^2$

- bogie yaw rate gyroscope: $1.44 * 10^{-6} rad^2/s^2$

- lateral distance between bogie and carbody: $4 * 10^{-6} m^2$

Considering these parameters, a number of simulations have been performed, in order to validate the control strategy. In Section 4.4 the results are displayed and compared with the LQ control strategy, as an ideal term of reference.

4.4   Linear simulation

As for the LQ control, the aim is to roughly recover the passive system performances; primary yaw stiffness is still reduced to the 10% of the original passive model value.

Moreover, it is interesting to compare these results with the LQ results, because the differences represent the validity of the Kalman estimation. Below, a number of simulation are presented, focusing on the perfomances degradation caused by the state estimation.

The red line is the LQ control and the blue line is the LQG control. The simulation characteristics are $v = 40$ m/s, $\lambda = 0.15$.
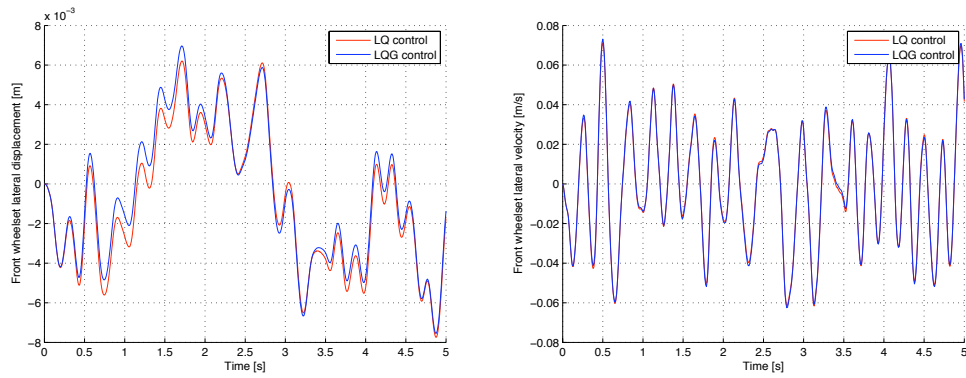
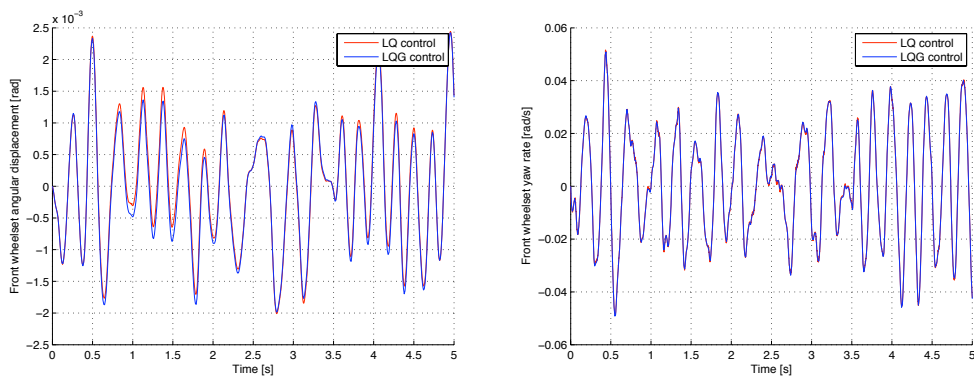Figure 4.3: Front wheelset lateral displacement and velocity

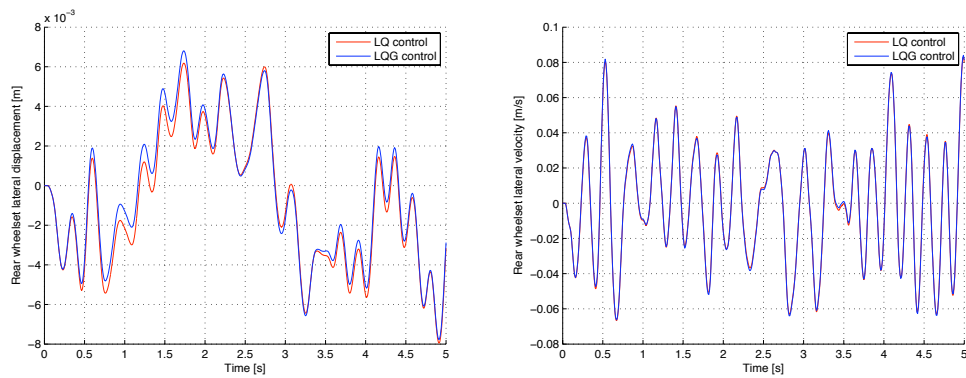Figure 4.4: Front wheelset angular displacement and yaw rate

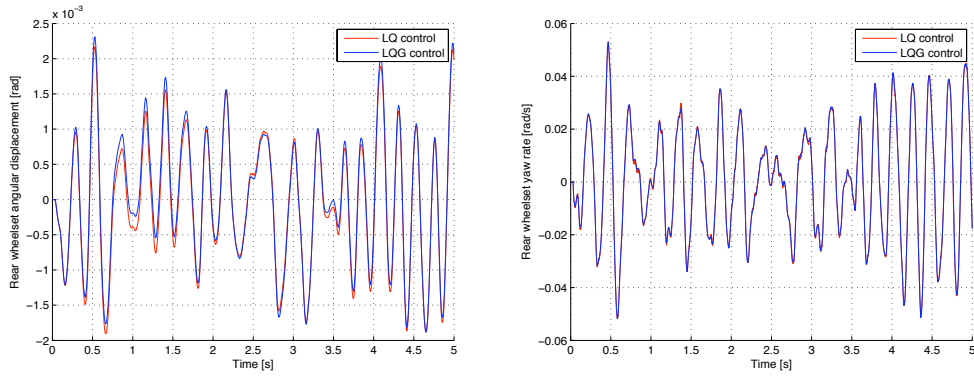Figure 4.5: Rear wheelset lateral displacement and velocity

43

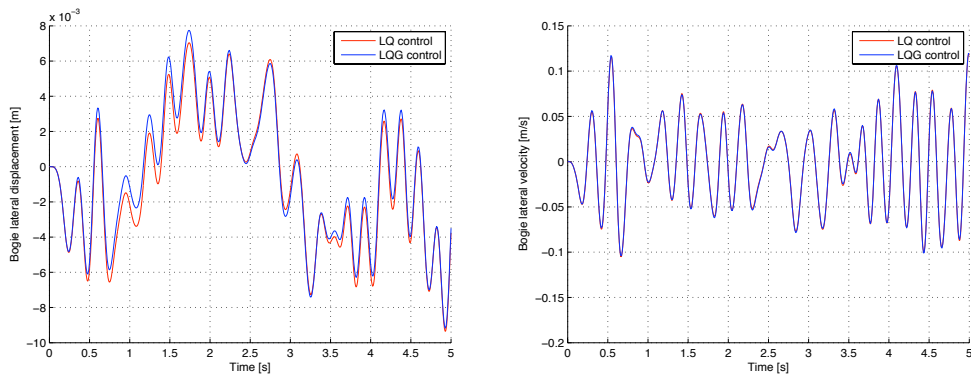*Figure 4.6: Rear wheelset angular displacement and yaw rate*

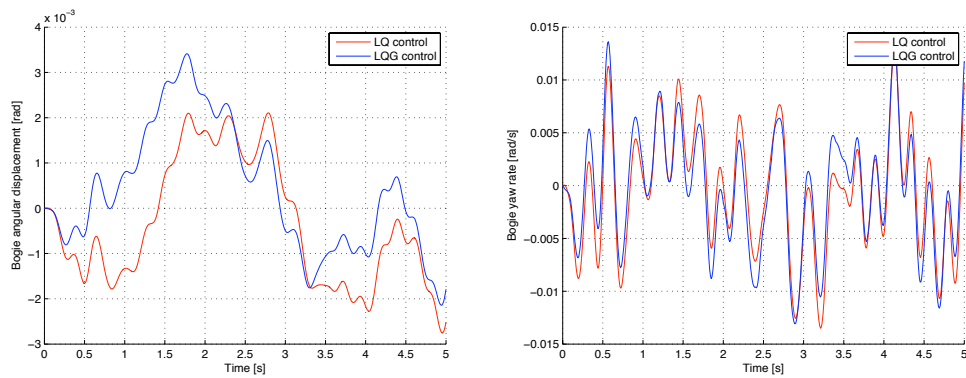*Figure 4.7: Bogie lateral displacement and velocity*

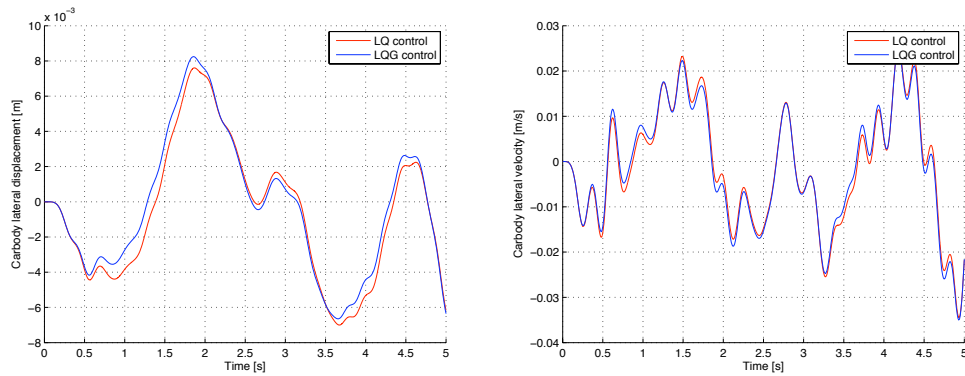*Figure 4.8: Bogie angular displacement and yaw rate*

44

Figure 4.9: Carbody lateral displacement and velocity

As it can be noticed in the figures, LQ and LQG control are very similar; this means that the Kalman filter has a good behaviour. The only two curves that show significant differences are in Figure 4.8, that is where the active control acts. This behaviour is sensible, and it is interesting to compare the two active control charts. Here it is condensed the differences between the full state measure and the Kalman estimation; since the curves are as previously very similar, it can be concluded that the state estimation works properly.

In the next chapter, the last part of the thesis is presented: a multi-body non-linear simulation of the control strategies developed on the linear model.

Chapter 5

Control strategy simulation with a multi-body non-linear model

5.1 Introduction

After having developed and tuned the control strategies on the linear model, the results are compared with a non-linear multi-body simulation. In this Chapter, only the LQ control strategy has been implemented, because of the long implementation of a state estimator in the multi-body simulator and the lack of time due to time constraints. It has been decided to assess the results with a more complicated and complete type of simulation mainly because the aim of the thesis can be validated only on a curved track. With a linear model is very difficult to represent the real dynamics of a curved track, because of several limitations:

- linear modellization of wheel rail contact mechanism

- complex curved track equation of motion writing

- non reliable results, due to the large semplification of the vehicle dynamics

Therefore, a non-linear multi-body simulation has been chosen because it better describes the reality. At Politecnico di Milano some multi-body models have been developed and used in past research programmes, hence in this work one of these models has been used to describe the vehicle studied in the linear model. In particular, the simulator taken into account is described in [10]. The multi-body model contains:

- a carbody, modelled as a single rigid body

- a bogie assembly, modelled as a rigid bogie frame connected by primary suspensions to two exible wheelsets

- other bodies attached either to a carbody or to a bogie frame (e.g. motors, converters etc.), modelled as rigid

These elementary units are connected to each other by elastic and damping elements (linear and nonlinear) reproducing the secondary suspensions and other elastic connections such as links between carbodies, elastic motor suspension etc. By combining the above listed elementary units, any specic trainset architecture may be derived; in the case studied in this work, a railway vehicle formed by two bogies and one carbody has been set up.

Each rigid body is assigned with five degrees of freedom, the forward speed of body centre of mass being set to a constant value V , whereas for each flexible wheelset, the movement with respect to the moving reference is dened as the linear combination of the unconstrained wheelset eigenmodes.

Besides the multi-body model construction, the other important parameter is the wheel-rail contact modellization. Both contact path geometry and creep coefficient have been considered as non linear. These assumptions imply a very different model of wheel-rail contact from the one used in the linear model described in Chapter 2. Therefore, a direct comparison of a time history between the linear and the non linear model would not be meaningful. For example, in Figure 5.1 the blue line represents the multi body simulation, the green line the linear simulation. The simulation characteristics are $v = 40\,m/s$, $\lambda = 0.025$. As it can be seen, the two lines follow the same
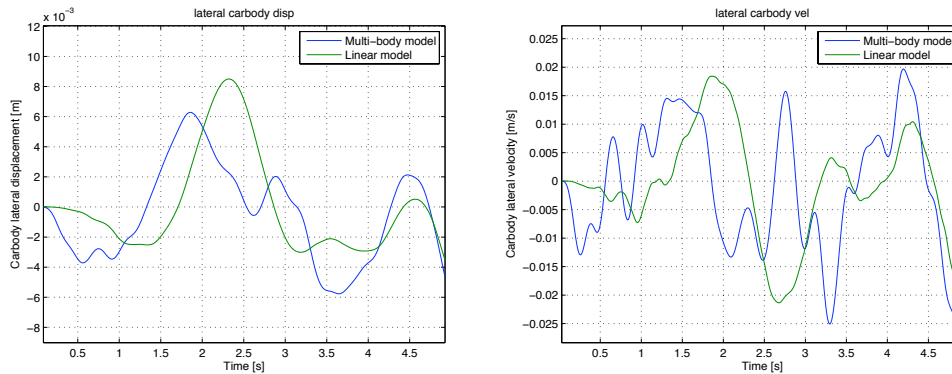
Figure 5.1: Carbody lateral displacement and velocity - comparison of linear and non-linear simulation for the passive vehicle

trend, but they are not very close. Therefore, multi-body simulation results will be compared only among themselves, hence will be compared the passive model, the passive model with the lowered primary yaw stiffnes, and the active model.

5.2   Simulation scenarios

In order to assess the performances of the system and to display the results, a number of different running situations have been simulated.

On straght track, the multi-body simulation has been performed with lateral track irregulaties, as done for the linear model. The vehicle speed is $v = 40\,m/s$.

Concerning to the curving situation, the simulations have been done without disturbances, in order to display better the behaviour of the system and then to make the comparisons easier. The simulation characteristics are $v = 31.5\,m/s$, curve radius $R = 500\,m$, non compensated lateral acceleration $a = 1\,m/s^2$, track cant $h = 150\,mm$.

For both the track situations, the configurations taken into account are:

- passive system

- passive system with lowered value of primary yaw stiffness

- active system

5.3 Simulation results

In this section the final results are displayed, focusing the attention on the curving performances related to the primary yaw stiffness.

5.3.1 Straight track results

In order to assess the straight track performances, a comparison on several stability indices has been done. The European norm EN14363 defines the boundaries in which the railway vehicle must be; in particular, one of those boundaries regards the maximum lateral acceleration of each wheelset. This information can be assumed as the safety limit for stability condition. This measure must be done with an accelerometer put on the axlebox of the wheelset.

The figures are generated to compare the behaviour of the three different models set up. As it can be clearly seen in Figure 5.2, the passive model with the lowered primary yaw stiffness exceeds the limit imposed by the norm. The other two models, conversely, stay below the threshold. The figures refer to the rear wheelset of the rear bogie; the simulations have been conduced with the same lateral irregularities used in the linear modellization. The red line refers to the RMS value of the lateral acceleration. It is interesting to compare this information because it assesses with a single parameter the performances of the system. In Table 5.1 the maximum RMS values are compared; the best performances are reached by the active controlled system.
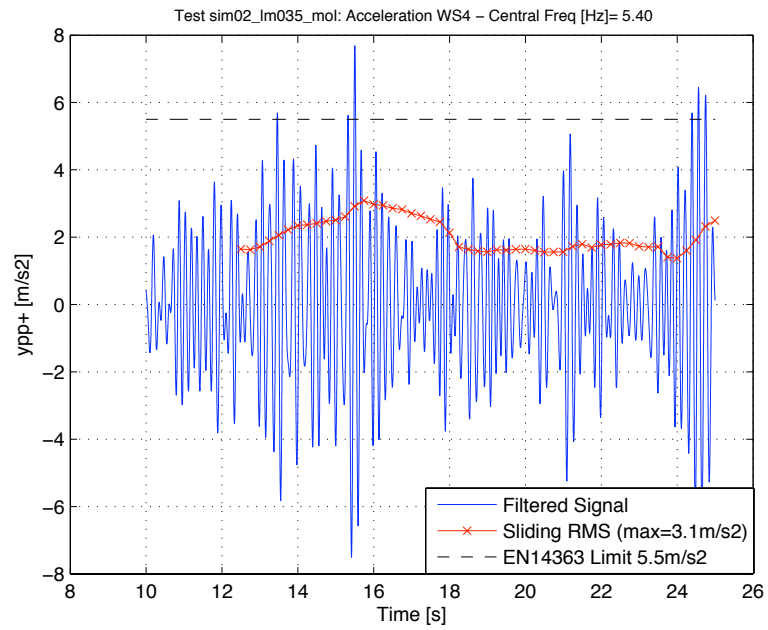
Figure 5.2: Passive model with the lowered primary yaw stiffness simulation

Passive with low p.y.s.	Passive	Active
$3.1\,m/s^2$	$2.1\,m/s^2$	$1.5\,m/s^2$

Table 5.1: Straight track lateral wheelset acceleration RMS values comparison
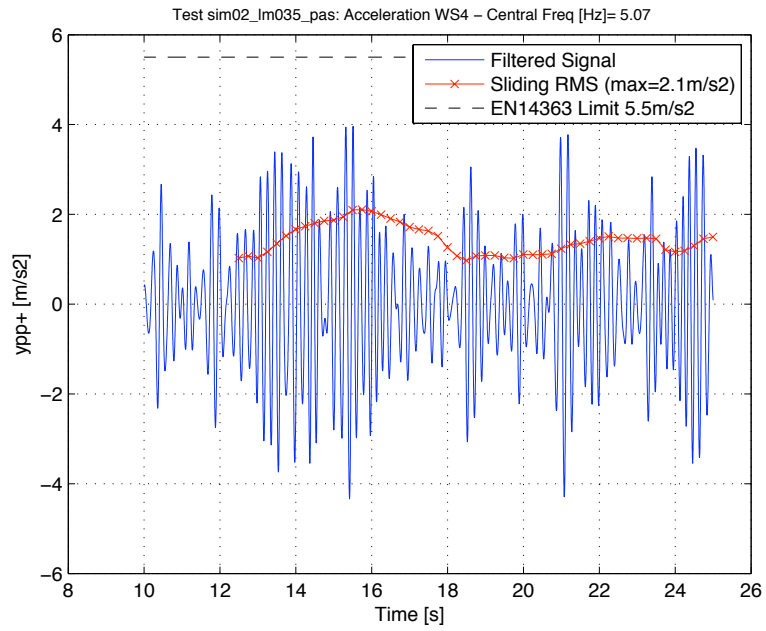
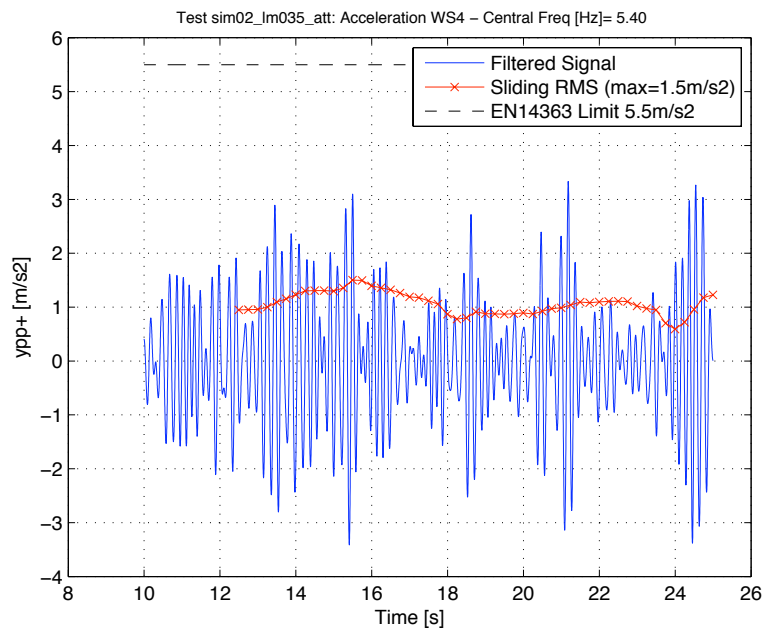*Figure 5.3: Passive model simulation*

Figure 5.4: Active model simulation

51

5.3.2 Curved track results

In curved track situation, the comparison criterion is different. Three different indices are taken into account:

- Y/Q ratio

- maximum track shift force

- wear index

These indices could be considered as indicators of the vehicle's running safety (the first two ones) and of the damage produced on the track (the third parameter). The first one describes the ratio between the lateral force and the vertical force acting on the external wheel; the second one measures the ripage forces, that are the sum of the lateral forces on the two wheels of the same wheelset; the last parameter is a measure of the work dissipated by the contact forces at one wheel. Wheel wear experiments have shown that the amount of wear taking place on the wheel and rail surface depends on the amount of work dissipated ([8]). For this reason, the parameter is called "wear index". The wear index is defined as

$$W_i = (\overrightarrow{T_i} \bullet \overrightarrow{\gamma_i}) * v \tag{5.1}$$

where $\overrightarrow{T_i}$ is the friction force on the $-i$ wheel expressed in N; $\overrightarrow{\gamma_i}$ is the creep coefficient on the $-i$ wheel; v is the vehicle speed expressed in m/s.

Therefore, the three indicators provide a comprehensive examination of running safety and of the wear generated on the wheels and on the infrastructure. Concerning to the first index, the external wheel of the leading wheelset has been taken into account, because it shows the maximum values. In fact, when the vehicle approaches a curve, the first wheelset tends to stay in straight position, and then it shows high creep forces. Figure 5.5 shows the time history of the Y/Q ratio for the three vehicle configurations considered.
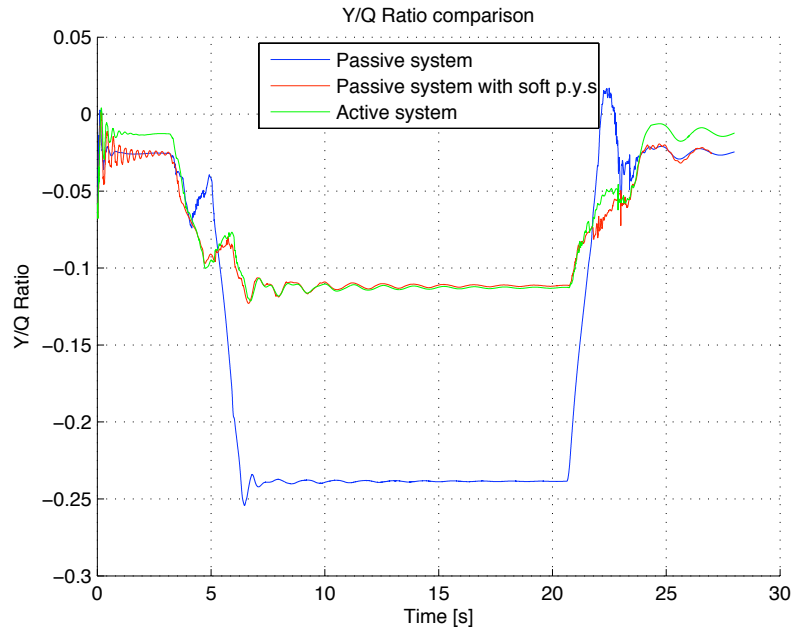
Figure 5.5: Y/Q Ratio comparison

It is observed that in the passive model, as expected, the Y/Q ratio is bigger than the other two models. Moreover, it is remarkable that the active model and the passive with the lowered primary yaw stiffness have the same behaviour, with slight differences. This is due to the fact that the simulation speed is much lower than the critical speed, hence the action of the active control is small.

The second index, regarding the ripage forces, measures the lateral force generated on the wheelset that affects the rail, and consequently might produce a shift of the track. The analysis has been conduced in the same way of the Y/Q ratio, except for the considered wheelset: the displayed results concerns to both wheelsets of the rear bogie. Returning to the concept of "perfect curving", the target is to equalize the ripage forces on the two wheelsets. As it can be seen in Figure 5.6, 5.6, 5.6, the passive model has relevant differences between the two ripage forces; on the contrary, a soft primary yaw connection reduces significantly the gap between the two lateral forces. Besides, it can be noticed that the behaviour of the active model is better
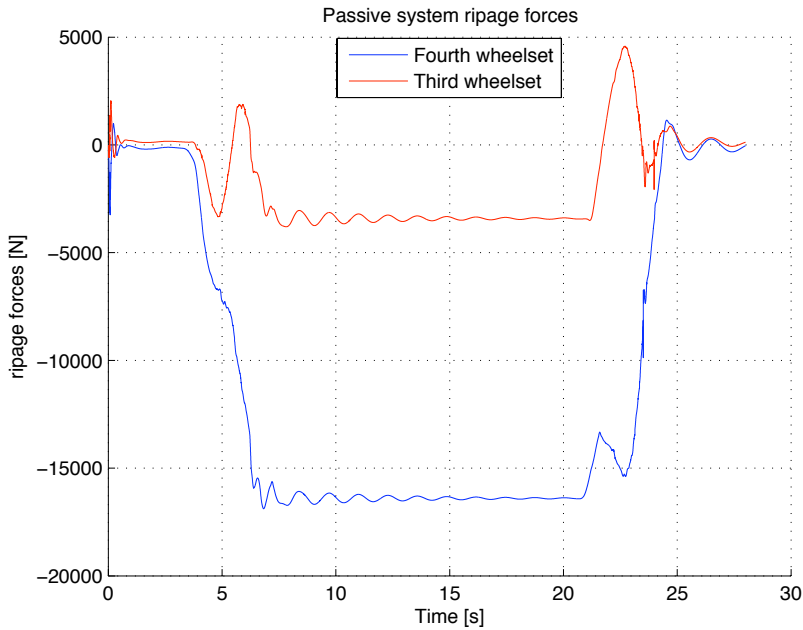
Figure 5.6: Passive model ripage forces

than the passive with the lower primary yaw stiffness; in particular, it has got reduced vibrations and more equalized ripage forces. In this case the control action works reducing the vibrations and steering the bogie towards the inside of the curve. In fact, when the vehicle is running on a curve, the bogie tents to stay in a understeer position, due to the dynamics of the system. Active control, in order to equalize the ripage forces, steers the bogie, obtaining a better result compared to the others.

Concerning to the wear index, the results are displayed as the power dissipation on each wheelset caused by the longitudinal and trasversal creep forces. Then the dissipated energy is displayed, computed as the integral of the power dissipation. The numerical results are summarized in Table 5.2, where the total dissipated energy on each wheel is listed; trasversal and longitudinal components have been summed. In the figures, the trailing wheelset of the rear bogie wheelset has been taken into account. As it can be clearly seen (Table 5.2), a drastic reduction of energy dissipation can be obtained using a soft primary yaw stiffness connection. Moreover, as seen for the ri-
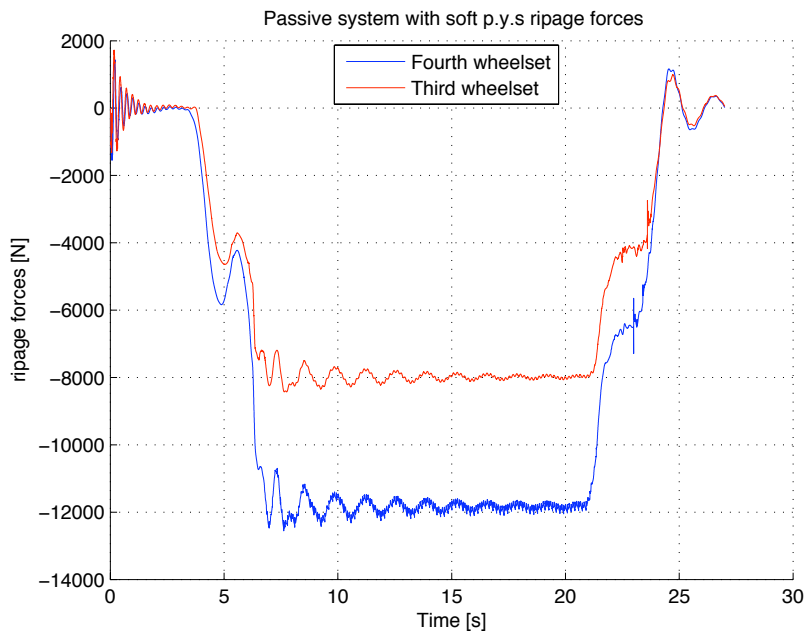
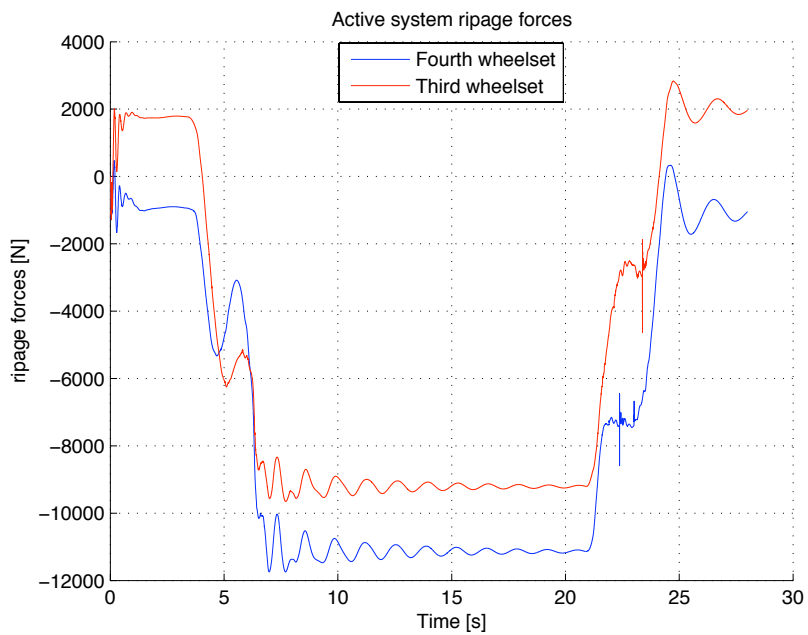Figure 5.7: Passive model ripage forces with soft p.y.s.

Figure 5.8: Active system ripage forces

page forces, the active control tents to reduce the vibrations (Figure 5.10, 5.11), and then better perfomances can be achieved.

Wheel	Passive	Passive with low p.y.s.	Active
1 R	132107 J	2271 J	2562 J
1 L	34500 J	4194 J	4619 J
2 R	4298 J	1554 J	1543 J
2 L	3918 J	1644 J	1618 J
3 R	111034 J	1338 J	2468 J
3 L	30493 J	2433 J	4531 J
4 R	6369 J	2772 J	1837 J
4 L	5525 J	2837 J	1840 J

Table 5.2: Energy dissipation on each wheel: the number refers to the wheelset (i.e. 2=trailing wheelset of the first bogie), the letter refers to Right or Left wheel
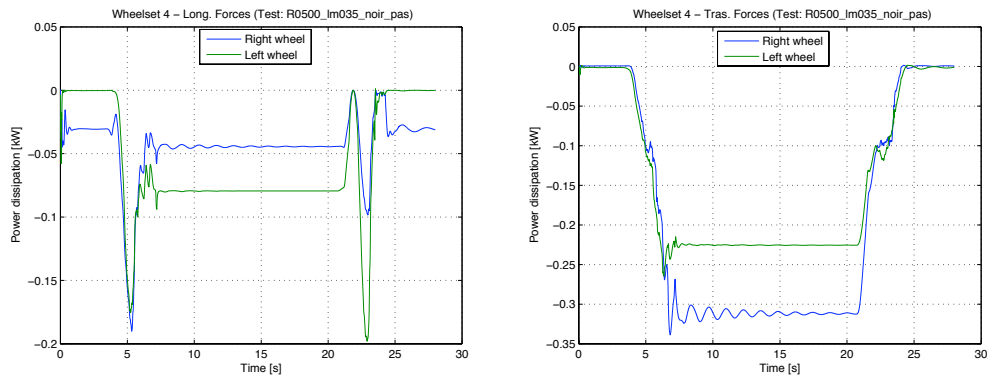

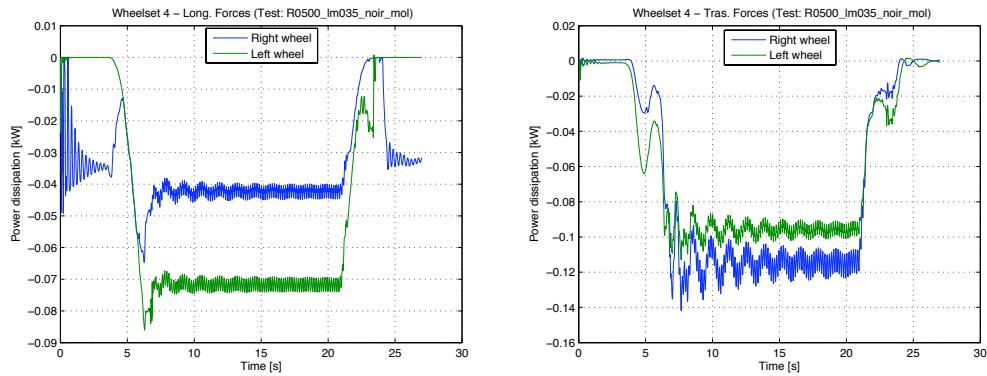*Figure 5.9: Power dissipation of the two wheels, passive model*

Figure 5.10: Power dissipation of the two wheels, passive model with soft p.y.s.
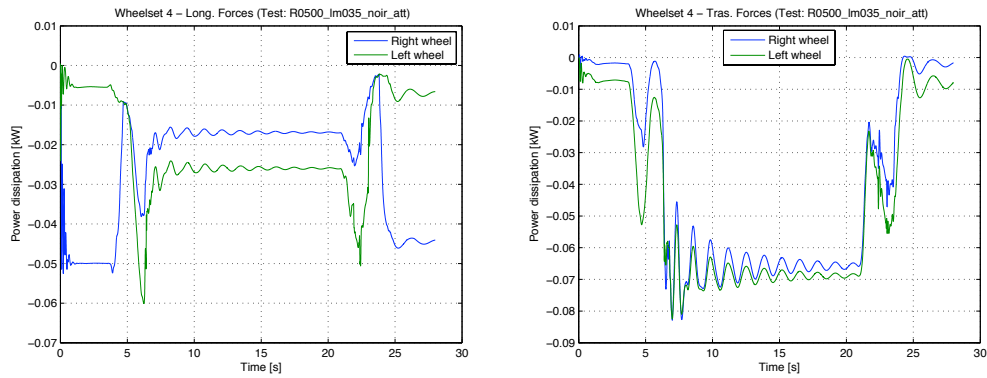

Figure 5.11: Power dissipation of the two wheels, active model

5.4 Multi-body simulations conclusions

In this Chapter a multi-body non-linear simulator has been used in order to test the performances of the different railway vehicle models taken into account in this thesis.

Firstly, a straight track test has been done in order to check the behaviour of the models on the multi-body simulator. Then, established the sensibleness of the results, some tests on curved track have been conduced. In particular, in order to assess the curving performances, three indices have been used: Y/Q ratio, track shift force and the wear index. With these three indices it was possible to validate the advatages of an active control applied on a

vehicle with soft primary yaw stiffness connection. The initial hypotesis of better curving performances have been verified and quantified by the test performed on the different models in different situations.

Chapter 6

Conclusions

In this study the potential improvements in curving performance through the use of a secondary yaw control has been presented. Curving performaces have been improved through a reduction of the primary yaw stiffness. Active control provides the needed stabilization, where a passive damper cannot give stability. The improved curving means less wear on the wheels and rails, and therefore lower maintenance costs. It also improves the running safety in a curve.

A linear half vehicle plan view has been developed in order to study the properties of the mechanical system, and to allow a control strategy development. Basically, two different types of inputs have been used, a lateral step input and a measured lateral track disturbance. Two different control strategies have been developed, an LQ full state control and an LQG control with state estimation. A sensing assessment has been done in order to describe the mechanical system equipped with the sensors.

The performances of the three different models (passive, LQ, LQG) have been firstly compared on the linear model, and then with a more precise multi-body non-linear simulator, which provides accurate results also for the curving condition. The simulations have been conduced both in straight and curved track, highlighting in every situation the advantages of an active control utilization.

Further reaserch, starting from this work, could be identified as:

- development of a different control strategy, for example an H_∞ approach

- a modellization of the actuator, in order to study the dynamic influence on the system

Bibliography

[1] Wickens A.H. Fundamentals of rail vehicle dynamics: guidance and stability. *Swets and Zeitlinger Publisher*, 2003.

[2] Bruni S Braghin F. and Resta F. Active yaw damper for the improvement of railway vehicle stability and curving performances: simulations and experimental results. *Vehicle System Dynamics Vol. 44, No. 11, November 2006, 857-869*, 2006.

[3] Mei T.X. Bruni S., Goodall R.M. and H. Tsunashima. Control and monitoring for railway vehicle dynamics. *Vehicle System Dynamics: International Journal of Vehicle Mechanics and Mobility, vol.45(7-8), Special Issue: State of the Art Papers of the 20th IAVSD Symposium, pp 743-779*, 2007.

[4] Diana G. and Cheli F. Dinamica e vibrazioni dei sistemi meccanici. *UTET Libreria*, 1993.

[5] Mirzapour M. Hubbard P., Mei T.X. and Ward C. Half cost trains: design for control. *Rail Research Association UK*, 2013.

[6] Suda Y. Michitsuji Y. Tanimoto M. Miyauchi E. Matsumoto A. Ohno H., Mizuma T. and Sato Y. Research on high curving performance trucksconcept and basic characteristics of active-bogie-steering-truck. *Vehicle System Dynamics, 41(suppl), 3342*, 2004.

[7] Goodall R.M. Persson R. and K. Sasaki. Carbody tilting - technologies and benefits. *Vehicle System Dynamics, 47(8), pp. 949-981*, 2009.

[8] Lewis R. and Olofsson U. Wheel-rail interface handbook. *Woodhead Publishing*, 2009.

[9] Goodall R.M. and Mei T.X. Kalman filters applied to actively controlled railway vehicle suspensions. *Transaction of the Institute of Measurement and Control, Vol. 23, No 3, 163-181*, 2001.

[10] Alfi S. and Bruni S. Mathematical modelling of trainturnout interaction. *Vehicle System Dynamics: International Journal of Vehicle Mechanics and Mobility, 47:5, 551-574*, 2009.

Appendix A

Symbols and parameters values

Symbol	Value	Parameter
v	40 [m/s]	Vehicle forward velocity
d	0.01 [m]	Lateral track step disturbance
r_0	0.45 [m]	Rolling radius
λ	0.15	Conicity
l	0.75 [m]	Half gauge
L	1.3 [m]	Semi wheelbase
D	0.45 [m]	Primary bush length
h_{ws}	1 [m]	Primary suspension lateral semi spacing
A_d	1.25 [m]	Semi spacing of longitudinal dampers
f_{11}	10e6 [MN]	Longitudinal creep coefficient
f_{22}	8.8e6 [MN]	Lateral creep coefficient
f_{23}	13.7e3 [MN]	Spin creep coefficient
f_{33}	0 [MN]	Spin creep coefficient
m_v	30000 [kg]	Carbody mass
m_b	2500 [kg]	Bogie mass
m_w	1120 [kg]	Wheelset mass
I_b	2500 [kgm^2]	Yaw inertia of the bogie
I_w	730 [kgm^2]	yaw inertia of the wheelset

I_{wy}	29.61 [kgm^2]	pitch inertia of the wheelset
W	96824.7 [N]	Wheelset load
k_{y1}	1000000 [N/m]	Primary lateral stiffness
k_{x1}	1000000 [N/m]	Primary longitudinal stiffness
f_{y1}	0 [Ns/m]	Primary lateral damping
f_{x1}	0 [Ns/m]	Primary longitudinal damping
k_{y1b}	4000000 [N/m]	bush lateral stiffness
k_{x1b}	14000000 [N/m]	bush longitudinal stiffness
f_{y1b}	0 [Ns/m]	Bush lateral damping
f_{x1b}	0 [Ns/m]	Bush longitudinal damping
k_{y2}	280000 [N/m]	Secondary lateral stiffness
f_{y2}	30000 [Ns/m]	Secondary lateral damping
k_{psi2}	50000 [Nm/rad]	Secondary yaw stiffness
f_{x2}	250000 [Ns/m]	Longitudinal yaw damping